



Antarctic Sea Ice Climatology, Variability, and Late Twentieth-Century Change in CCSM4

LAURA LANDRUM, MARIKA M. HOLLAND, AND DAVID P. SCHNEIDER

National Center for Atmospheric Research, Boulder, Colorado

ELIZABETH HUNKE

Los Alamos National Laboratory, Los Alamos, New Mexico

(Manuscript received 9 May 2011, in final form 27 January 2012)

ABSTRACT

A preindustrial control run and an ensemble of twentieth-century integrations of the Community Climate System Model, version 4 (CCSM4), are evaluated for Antarctic sea ice climatology, modes of variability, trends, and covariance with related physical variables such as surface temperature and sea level pressure. Compared to observations, the mean ice cover is too extensive in all months. This is in part related to excessively strong westerly winds over $\sim 50^{\circ}$ – 60° S, which drive a large equatorward meridional ice transport and enhanced ice growth near the continent and also connected with a cold bias in the Southern Ocean. In spite of these biases in the climatology, the model's sea ice variability compares well to observations. The leading mode of austral winter sea ice concentration exhibits a dipole structure with anomalies of opposite sign in the Atlantic and Pacific sectors. Both the El Niño–Southern Oscillation and the southern annular mode (SAM) project onto this mode. In twentieth-century integrations, Antarctic sea ice area exhibits significant decreasing annual trends in all six ensemble members from 1950 to 2005, in apparent contrast to observations that suggest a modest ice area increase since 1979. Two ensemble members show insignificant changes when restricted to 1979–2005. The ensemble mean shows a significant increase in the austral summer SAM index over 1960–2005 and 1979–2005 that compares well with the observed SAM trend. However, Antarctic warming and sea ice loss in the model are closely connected to each other and not to the trend in the SAM.

1. Introduction

The Antarctic sea ice cover undergoes a large seasonal range from a climatological maximum of approximately 19 million km² in extent in September to a minimum of 3 million km² in February (e.g., Cavalieri and Parkinson 2008) (Fig. 1). The seasonal cycle of ice advance and retreat is influenced by the dominant seasonality in the atmosphere and the semiannual oscillation (SAO)—a biannual (spring and autumn) strengthening and poleward migration of the circumpolar trough (e.g., van Loon 1967; Enomoto and Ohmura 1990; Simmonds 2003; Stammerjohn et al. 2003; Simmonds et al. 2005). On an annual basis, considerable ice growth occurs near the continent with equatorward transport and subsequent melting at lower latitudes.

However, observational constraints on the Antarctic sea ice mass budgets are limited due in part to the remoteness of the region and the difficulties in observing sea ice thickness from satellites. The ice melt and growth cycles and associated freshwater fluxes can have important implications for ocean stratification and deep and intermediate water formation with consequent impacts on climate, biogeochemical cycling, and carbon sequestration (e.g., Smith and Nelson 1985; Takahashi et al. 2002; Zhang 2007; Arrigo et al. 2008; Kirkman and Bitz 2010).

In contrast to the Arctic, large-scale trends in Antarctic sea ice cover have been small and slightly increasing since satellite records began in 1979 (e.g., Cavalieri and Parkinson 2008). This small change is due to regionally compensating trends that are present since 1979. Significant ice loss has been observed in the Bellingshausen–Amundsen Sea extending into the western Weddell Sea, with compensating increases in the Ross Sea sector (Liu et al. 2004; Cavalieri and Parkinson 2008; Comiso and Nishio 2008).

Corresponding author address: L. Landrum, P.O. Box 3000, Boulder, CO 80307.
E-mail: landrum@ucar.edu

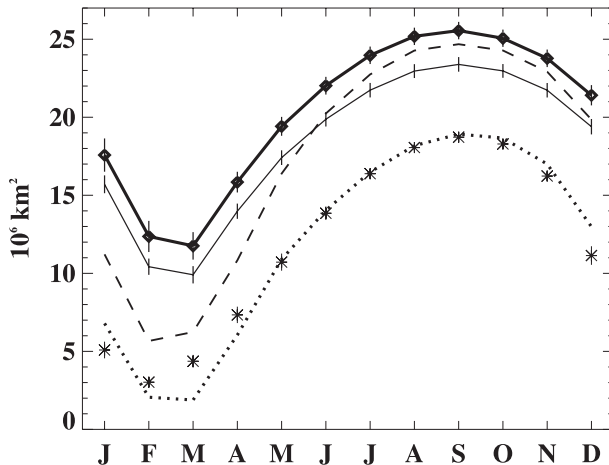


FIG. 1. The annual cycle of Antarctic sea ice extent from the CCSM4 PI integration (thick solid), the late twentieth-century (1979–2005) CCSM4 ensemble average (thin solid), the late twentieth-century CCSM3 average (dashed), and the hindcast ice-ocean simulation (dotted). Satellite-derived observations (Fetterer et al. 2009) are shown by the asterisks.

Over the observational record, Antarctic ice cover has exhibited coherent variations on interannual and longer time scales. Previous work has shown that this variability has a dipole structure with anomalies of opposite sign in the Atlantic and Pacific basins (Yuan and Martinson 2000). This “Antarctic dipole” has corresponding anomalies in surface ocean characteristics and atmospheric fields. Additionally, work suggests that winter anomalies of sea ice are collocated with anomalies in sea surface temperature, sea level pressure, and wind stress and can propagate around the Antarctic continent (White and Peterson 1996). The sea ice anomalies re-emerge from one year to the next because of an imprint of the winter ice conditions on the ocean surface temperatures (Gloersen and White 2001).

Variability and change in the Antarctic sea ice is associated with large-scale modes of atmospheric variability, most importantly the El Niño–Southern Oscillation (ENSO) and the southern annular mode (SAM) (e.g., Simmonds and Jacka 1995; Yuan and Martinson 2000; Liu et al. 2004; Yuan and Li 2008). Many observational studies suggest that ENSO initiates Southern Hemisphere (SH) variability, including modulation of the SAO, and that ice–ocean coupling prolongs the anomalies (e.g., Harangozo 1997; Peterson and White 1998; Yuan and Martinson 2000; Cai and Baines 2001; Yuan and Martinson 2001; Stammerjohn et al. 2003; Yuan and Li 2008). The influence of SAM variations on Antarctic sea ice has been documented in both observational (Stammerjohn et al. 2008) and modeling (Hall and Visbeck 2002; Holland and Raphael 2006; Sen Gupta and England 2006) studies.

The Southern Ocean plays a critical role in global ocean circulation as well as global cycling of carbon and nitrogen. Three climatologically important water masses are formed in the Southern Ocean: Antarctic Intermediate Water (AAIW), Subantarctic Mode Water (SAMW; both formed near and north of the Antarctic Circumpolar Current), and Antarctic Bottom Water (AABW; formed over continental shelves along the Adelie coast and in the Ross and Weddell Seas). These water masses form as a result of complex interactions of atmosphere–ocean–cryosphere processes. Despite its relatively small surface area (~10% of the global ocean), 20%–30% of oceanic uptake of CO₂ occurs in this area (Takahashi et al. 2002). AABW carries some of the deepest and highest concentrations of anthropogenic CO₂ in the world’s oceans (e.g., Lo Monaco et al. 2005)—uptake that is heavily influenced by physical and biological conditions in the surface ocean. Interannual variability in Southern Ocean productivity is most closely related to variability in sea ice (Arrigo et al. 2008). To effectively use climate models to investigate Southern Ocean processes, an assessment of Antarctic sea ice conditions and variability is needed. Previous modeling studies have diagnosed variability in sea ice and its relationship to large-scale modes of atmospheric variations (e.g., Hall and Visbeck 2002; Holland et al. 2005; Sen Gupta and England 2006). These studies suggest that climate models can reasonably simulate Antarctic sea ice variability and provide considerable insight into the mechanisms driving those variations.

The Community Climate System Model, version 4 (CCSM4), is a new model with significant improvements across all model components as compared to previous model versions (Gent et al. 2011). Here we assess the Antarctic sea ice simulation within CCSM4 preindustrial and twentieth-century integrations. This includes a description of the simulated Antarctic sea ice and analysis of the linkages between the sea ice and other Southern Ocean–atmosphere fields and global climate indices in CCSM4. We describe both the mean state and model variability from a nontransient preindustrial (year 1850) control run. Mechanisms driving simulated sea ice variability and linkages to large-scale modes of atmospheric variability are discussed. We then investigate sea ice changes in transient twentieth-century model runs from six ensemble members including the seasonality of simulated sea ice change and provide comparisons to observed twentieth-century change.

2. Experiments and observational data

We assess the Antarctic sea ice mean state, variability, and change in simulations from the CCSM4 and provide some comparisons to the previous model version (CCSM3; Collins et al. 2006). For further aspects of the CCSM3

simulated Antarctic sea ice and atmosphere see Holland and Raphael (2006) and Raphael and Holland (2006).

The CCSM4 is a fully coupled climate model as described by Gent et al. (2011). The atmospheric component uses the Community Atmospheric Model version 4 (Neale et al. 2012, manuscript submitted to *J. Climate*), which employs a finite-volume grid at a horizontal resolution of about $1^\circ \times 1^\circ$ and with 26 vertical levels. The land model, which is run on the same horizontal grid as the atmosphere, is the Community Land Model version 4 (CLM4; Lawrence et al. 2012). The ocean model component is described in Danabasoglu et al. (2012) and is based on the Parallel Ocean Program (POP) of the Los Alamos National Laboratory (Smith et al. 2010). The sea ice component uses the Los Alamos National Laboratory Sea Ice Model, version 4 (Hunke and Lipscomb 2008). Major updates of the ice model compared to CCSM3 are discussed in Holland et al. (2012). This includes improvements in the physical representation of the albedo treatment, including the incorporation of melt pond and aerosol deposition effects, and generally more realistic snow-covered albedo values (Gent et al. 2011). Both the ice and ocean model use a nominally 1° grid, which has a north pole that is smoothly displaced into Greenland.

To study CCSM4 Antarctic sea ice variability and mean state in the absence of transient forcings, we analyze model output for 500 yr of a 1300-yr preindustrial integration (simulation years 701–1200 of the 1850 control run). The 1850 control run is a fully coupled land–ocean–ice–atmosphere run that is forced at constant 1850 conditions (constant trace gases, land use and plant functional types, orbital parameters and solar irradiance, and aerosols), and described in more detail by Gent et al. (2011). Output from the control simulation, forced by preindustrial conditions (and hence termed “PI”) is used to initialize the twentieth-century simulations. The PI also provides a simulation from which to compare internal model variability to external variability resulting from twentieth-century transient forcings.

Twentieth-century Antarctic variability and change is assessed from the 1850–2005 ensemble integrations, primarily focusing on the period since 1960 for its overlap with Antarctic instrumental observations. The twentieth-century simulations are initialized from years in the PI run that are chosen to span the range of variability observed in the North Atlantic meridional overturning circulation. They are forced by natural and anthropogenic forcings (Gent et al. 2011), including time-varying greenhouse gas concentrations, time- and space-varying stratospheric and tropospheric ozone, black and primary organic carbon aerosols, direct effect of sulfate aerosols (indirect effects were not included),

and land use and land cover change (Lawrence et al. 2012). The Community Atmospheric Model version 3.5 was used offline with a fully interactive chemistry model to compute decadal-average monthly three-dimensional concentrations of ozone and aerosols (Lamarque et al. 2011) from historical emissions (Lamarque et al. 2010). Natural forcings for the twentieth century runs include volcanic aerosols (Ammann et al. 2003) and solar variability (Lean 2000; Wang et al. 2005). Further details of the twentieth-century runs and the climate response of CCSM4 can be found in Meehl et al. (2012). The individual twentieth-century ensemble members have tags 005, 006, 007, 008, 009, 010, and 011 that we retain in this paper so that interested researchers may identify the correct runs and to maintain consistency with other publications.

Climatology from the coupled experiments is compared to an ice–ocean coupled hindcast integration forced with interannually varying atmospheric data. The atmospheric forcing used is that available from the Coordinated Ocean–Ice Reference Experiments (CORE; Griffies et al. 2009) and encompasses the years 1948–2007. Details of the forcing are documented in Large and Yeager (2009). The model has been run through six cycles of the forcing and we analyze years corresponding to 1979–2005 from the last cycle. Ocean characteristics from this simulation are discussed in Danabasoglu et al. (2012).

The observational data that we use to evaluate the CCSM4 include climatological sea ice concentrations from the Special Sensor Microwave Imager (SSM/I) dataset (Comiso 1990), obtained from the National Snow and Ice Data Center (NSIDC) (<http://nsidc.org/data/nsidc-0002.html>), available as monthly or daily values. We also use the NSIDC’s Sea Ice Index (Fetterer et al. 2009), which contains monthly values of sea ice extent and sea ice area (http://nsidc.org/data/seaice_index/). For time-varying sea ice concentration we use the compilation of Hurrell et al. (2008). The Hurrell et al. dataset is a blend of optimally interpolated sea surface temperatures (SSTs) and sea ice (Reynolds et al. 2002) and of the Hadley Centre Sea Ice and SST dataset (HadISST) (Rayner et al. 2003) and was obtained online (<http://cdp.ucar.edu/MergedHadleyOI>). For surface temperatures, we use the 1200-km version of the Goddard Institute for Space Studies (GISS) Surface Temperature Analysis (GISTEMP) (Hansen et al. 2010). The GISTEMP analysis uses more Antarctic station data (Turner et al. 2004) than other global temperature analyses and makes interpolations across large distances, covering much of the Antarctic ice sheet and adjoining Southern Ocean. For sea level pressure (SLP), we use the globally complete, $5^\circ \times 5^\circ$ latitude–longitude gridded dataset, Hadley Centre SLP version 2 (HadSLP2; Allan and Ansell 2006). The GISTEMP and HadSLP2 data were obtained

from the Physical Science Division of the National Oceanic and Atmospheric Administration (NOAA) Earth System Research Laboratory, Boulder, Colorado (<http://www.esrl.noaa.gov/psd/data/>). Finally, a monthly index of the SAM is used from Marshall (2003) (obtained online from <http://www.antarctica.ac.uk/met/gjma/sam.html>).

3. Climatology

To diagnose the climatological sea ice state simulated by CCSM4, we analyze a 500-yr average of monthly output from the preindustrial control simulation. This is compared to conditions simulated by the ice–ocean hindcast integration and by CCSM3. Where possible, comparisons to observations are also discussed. Because observational records from satellite data are only available for about the last 30 yr, direct comparisons are confounded by the difference in time period and the different external forcings associated with these time periods. However, as discussed below, the biases compared to observed conditions are almost certainly larger than any large-scale changes that we expect have occurred since 1850. We will return to this point when discussing the sea ice changes simulated by the model over the twentieth century.

The simulated annual cycle of Antarctic sea ice extent is shown in Fig. 1. Consistent with observations, the ice cover undergoes a very large annual cycle, retreating from a maximum in September to a minimum in March. However, as compared to satellite observations the ice cover is too extensive throughout the year, with an annual average of 20.3 km² compared to 12 km² in the observations. Extensive Antarctic sea ice is also present in CCSM3, particularly in winter. However, CCSM3 simulates a larger annual cycle and reduced summer ice cover compared to the newer model (Fig. 1). Many changes are present between the CCSM3 and CCSM4 models (Gent et al. 2011), and it is difficult to attribute the simulation differences to a single model change. However, we do note that the sea ice albedo treatment is completely different in the new model (Holland et al. 2012) and CCSM4 simulates higher (and more realistic) albedos for snow-covered sea ice (Gent et al. 2011). Additionally, the “freeze-dry” parameterization (Vavrus and Waliser 2008) incorporated in CCSM4 reduces low cloud cover amounts in cold high-latitude conditions. As such, CCSM4 simulates considerably less low cloud cover in the Southern Ocean (not shown), particularly in winter, resulting in less year-round incoming longwave and enhanced summer shortwave radiation at the surface. These flux differences also contribute to differences in sea ice mass budgets between CCSM3 and CCSM4.

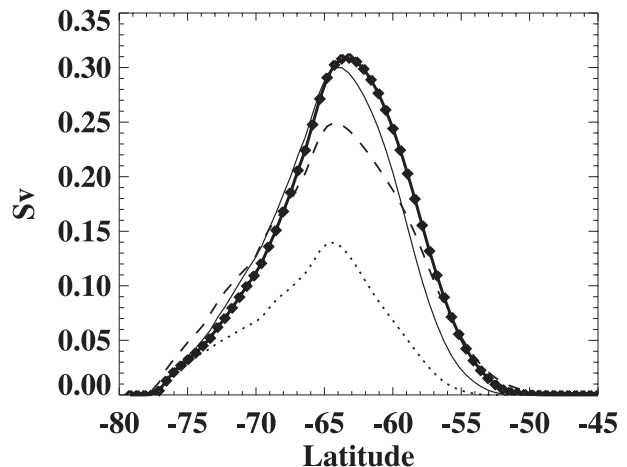


FIG. 2. The annual zonal mean meridional ice transport from the CCSM4 PI run (thick solid), the late twentieth-century (1979–2005) CCSM4 ensemble average (thin solid), the late twentieth-century CCSM3 average (dashed), and the hindcast ice–ocean simulation (dotted).

Multiple and interacting factors are likely responsible for the extensive CCSM4 sea ice, and consistent biases exist in the ocean simulation (Weijer et al. 2012). However cause and effect are difficult to determine. In the hindcast ice–ocean coupled simulations, the Antarctic sea ice shows more fidelity to observations and has a reasonable annual cycle (Fig. 1). Antarctic sea ice extent is also greatly improved in simulations with the CCSM4 configured with lower horizontal resolution ($\sim 3.75^\circ$ atmosphere; 3° ocean). These simulations have approximately 30% smaller zonal mean wind speeds in the Southern Ocean (Shields et al. 2012). This suggests that biases in simulated atmospheric fields are in part responsible for the sea ice bias. One such notable bias is that the Southern Ocean zonal wind stress from about 50° to 60° S is anomalously strong (by $>30\%$) compared to reanalysis products (Danabasoglu et al. 2012). [A similar bias is present in CCSM3 (Holland and Raphael 2006).] This is consistent with excessive equatorward Ekman ocean and sea ice drift, which likely contributes to cold temperatures and a biased ice extent. Observations of ice volume transport are limited and generally confined to small regions (e.g., Harms et al. 2001) making a comparison to the model results difficult. However, the zonal-mean meridional sea ice transport in CCSM4 (Fig. 2) is over twice as large as that simulated by the ice–ocean hindcast integration and is larger at its maximum than in CCSM3. Thus, it appears quite excessive. The net equatorward transport of sea ice is replaced near the continent by sea ice growth during the winter. In turn, the transported ice melts near the ice edge, resulting in a net equatorward transport of water

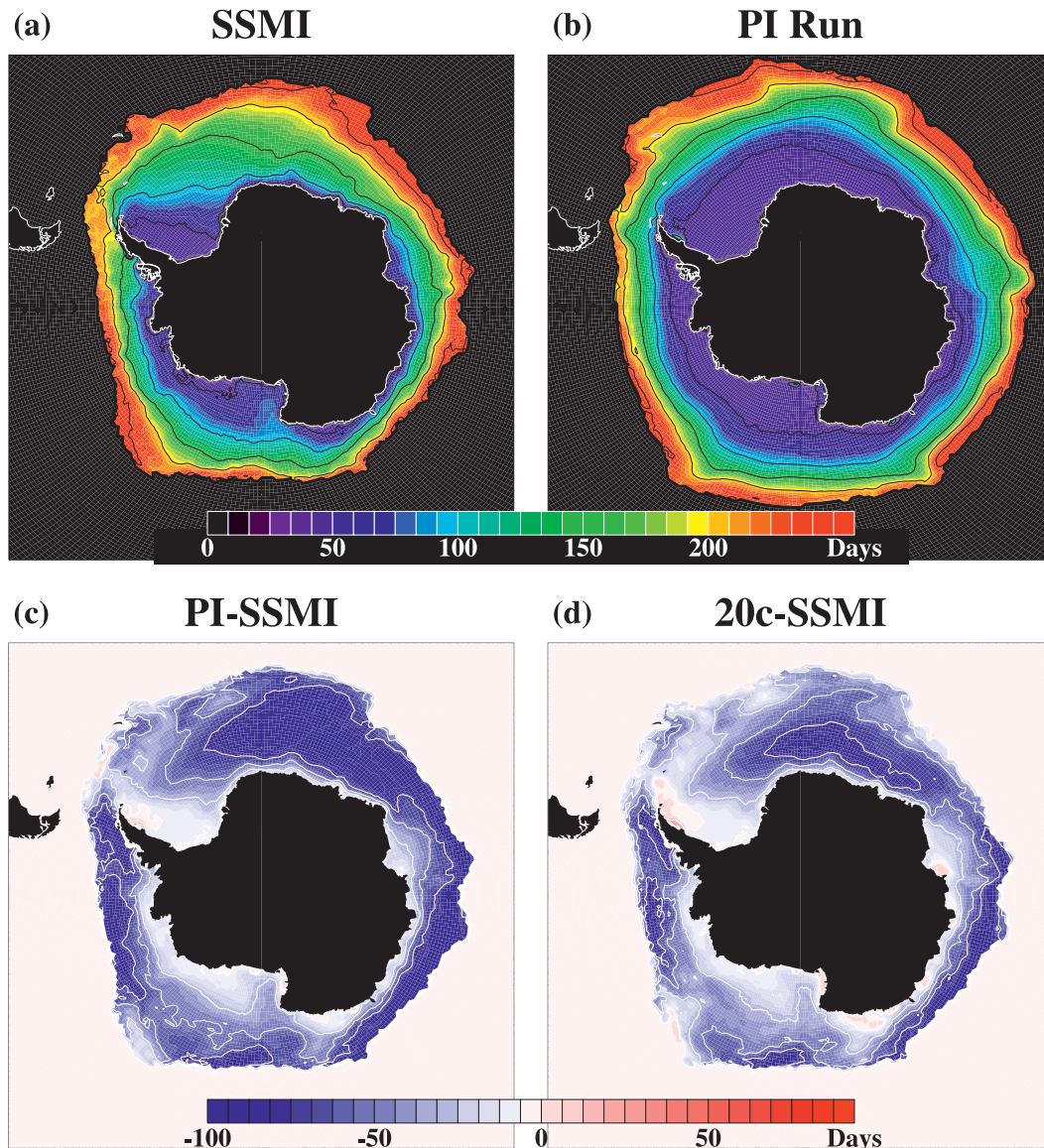


FIG. 3. Day of ice advance from (a) satellite observations, (b) CCSM4 1850 control run, and differences between (c) CCSM4 1850 control run and (d) twentieth-century ensemble mean and observations.

with implications for ocean buoyancy forcing and circulation as further discussed in Weijer et al. (2012).

Regional aspects of the ice concentration annual cycle can be quantified by the timing of ice advance and retreat. The difference between the advance and retreat dates gives information on the ice-season duration. These characteristics of the Antarctic sea ice pack have been effectively used in previous work (Parkinson 2002; Stammerjohn et al. 2008) to assess controls on Antarctic sea ice variability. Gridded daily averaged sea ice concentration (SIC) is available for 155 yr of the control simulation (years 953–1007) and is used to compute the date of ice advance and retreat. The ice advance date is

defined as the first day after 16 February for which ice concentration increases above 15% for five or more consecutive days. The date of ice retreat is similarly defined as the first day the ice concentration falls below 15% and remains below 15% until the end of the “ice year” (defined to be 15 February of the following calendar year). Ice duration in days is then the date of retreat minus the date of ice advance.

An analysis of daily satellite observations (Comiso 1990, updated) that have been interpolated to the model grid is also provided for comparison. The simulated mean timing of ice advance is shown in Fig. 3. Compared to the analysis of satellite observations, the simulated

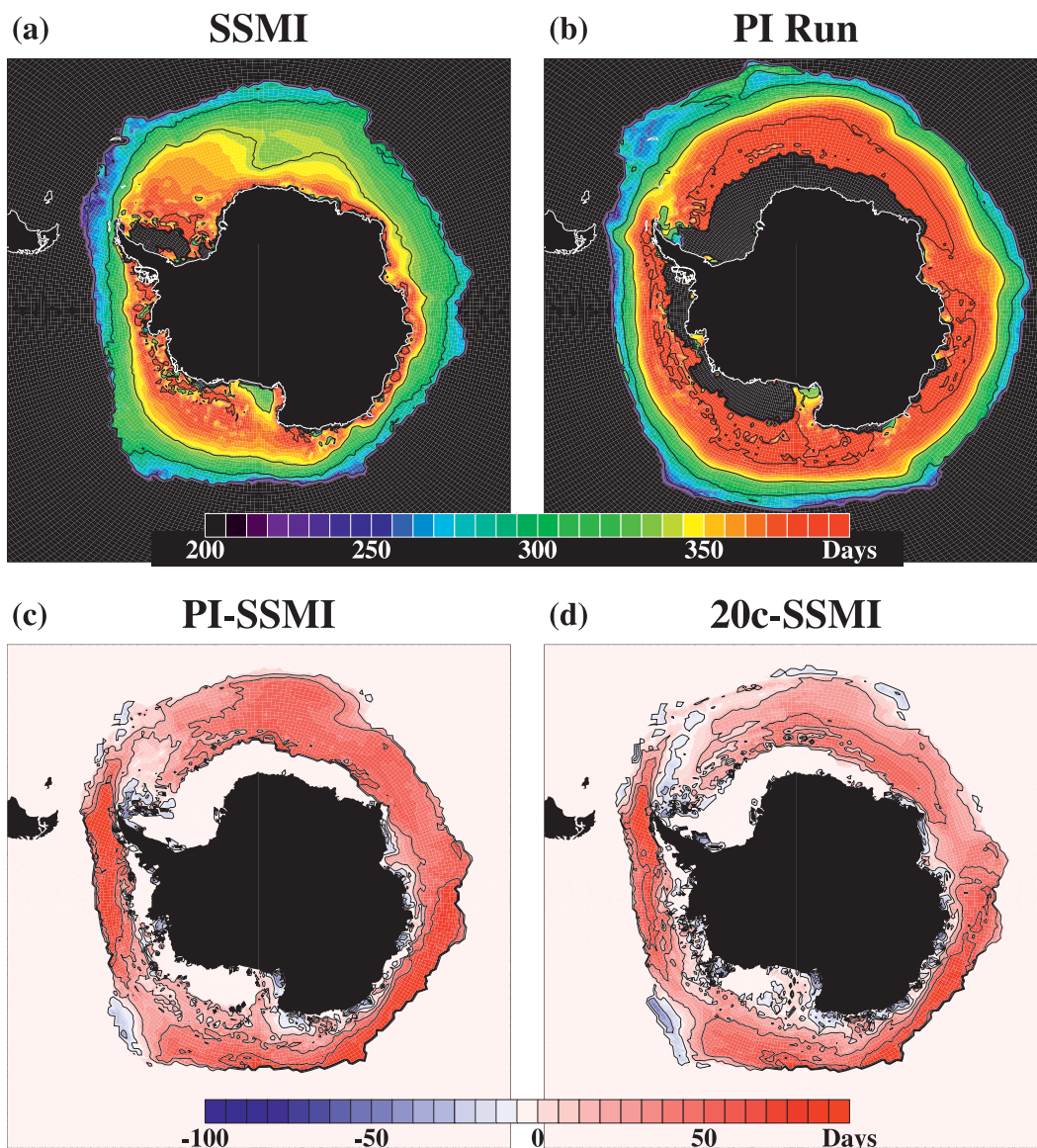


FIG. 4. Day of ice retreat in (a) SSMI observations, (b) CCSM4 1850 control run, and differences between (c) CCSM4 1850 control run and (d) twentieth-century ensemble mean and observations.

advance of the ice edge occurs too early, by up to 50 days over vast regions of the southern polar ocean. The bias is particularly large and widespread in the eastern Atlantic sector of the Southern Ocean. A comparison to simulated late twentieth-century conditions decreases this bias marginally (Fig. 3d). The timing of ice edge retreat (Fig. 4) is late in the model simulations by 50 or more days over large areas, again showing modest improvement when considering late twentieth-century-simulated conditions.

The biases in the timing of ice advance and retreat contribute to an excessively long ice-season duration, which is reflected in the spatial pattern of the ice concentration (Fig. 5). In general, anomalously high ice cover is

present in the model simulations throughout the Southern Ocean. In summer, too little melt back is simulated, and ice cover remains high. These biases have consequences for the simulated ice–ocean–atmosphere interactions and secular trends over the twentieth century, a point that we return to below.

4. Natural variability

a. Sea ice variability

Variability in the length of the ice-covered season (Fig. 6) is concentrated in the seasonal ice zone near the

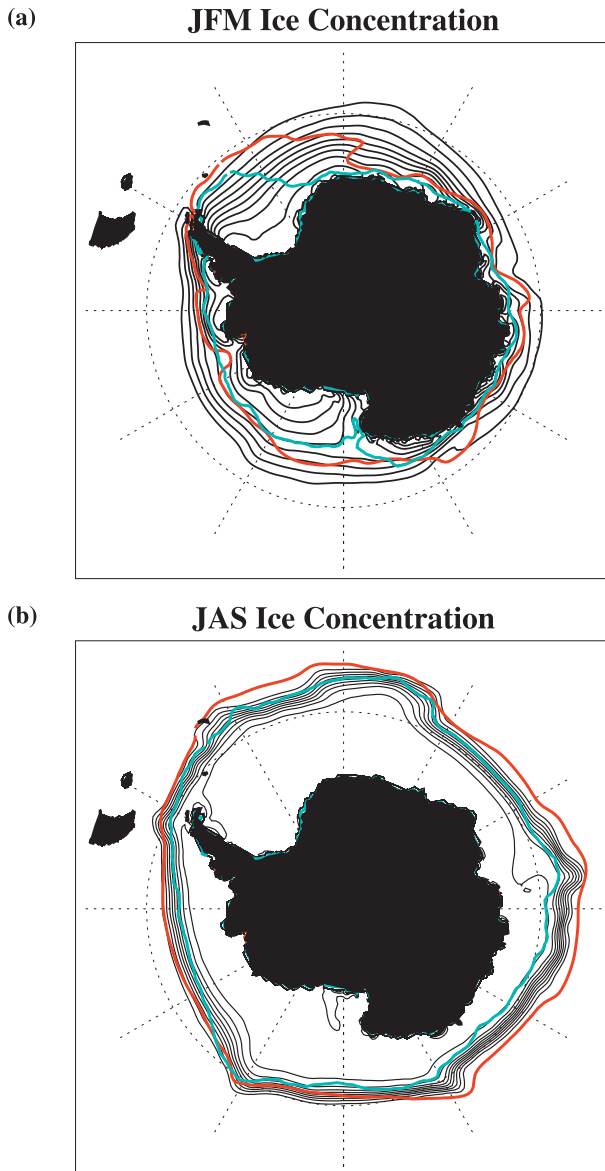


FIG. 5. The 1979–2005 ensemble mean CCSM4 SIC (black contours) in (a) austral summer [January–March (JFM)] and (b) austral winter (JAS). The contour interval is 0.1. The red contour corresponds to the 0.1 contour from the late twentieth-century CCSM3 results, and the blue contour corresponds to the 0.1 contour from 1979–2005 satellite data (Comiso 1990, updated).

ice pack edge. It has particularly large standard deviations in the Atlantic and Pacific sectors of the Southern Ocean. Variability in ice duration is related to anomalies in the date of ice advance and/or retreat. As shown in Fig. 6, anomalies in the ice advance timing are largest in the Pacific, whereas the timing of ice retreat is variable throughout the Atlantic, Pacific, and extending into the Indian Ocean sectors. This suggests that different processes may determine the ice anomalies in the

Pacific and Atlantic regions and is discussed further in section 4b.

The ice-season length variations are strongly associated with variability in the winter average sea ice concentration. To characterize the spatial and temporal structure associated with this winter Antarctic sea ice concentration variability, an empirical orthogonal function (EOF) analysis is performed. The long-term monthly means are removed from monthly fields before calculating any seasonal or annual means. The spatial patterns associated with each EOF are presented by taking the standardized principal component (PC) time series of the given EOF and regressing the original field onto the PC to result in a map with original units per standard deviation (e.g., percentage for sea ice concentration). Only modes that are distinct from each other according to the separation criteria of North et al. (1982) are presented (e.g., the first two modes of winter sea ice cover and annual surface temperature, and annual depth-integrated ocean temperature, and the first mode of annual sea level pressure). We focus on the austral winter [July–September (JAS)] average for ice fields, which is most closely related to the variations in ice-season length.

The two leading modes of winter SIC variability obtained from an EOF analysis are shown in Fig. 7. The leading EOF has a strong dipole pattern, with anomalies of opposite sign in the Pacific and Atlantic sectors. The anomaly centers coincide quite closely with anomalies associated with the leading mode of variability from observations (black contours on Fig. 7a) but are displaced somewhat equatorward consistent with biases in the mean state. The simulated leading mode of winter sea ice variability accounts for 25% of the variance in the winter SIC field (and also 25% in the observations). This simulated variability is similar to the “Antarctic dipole” in sea ice that is present in observations (Yuan and Martinson 2000). This suggests that the model may be reasonably capturing the longitudinal spatial structure of sea ice variability even with the biases in the mean state.

The second mode of winter SIC variability, accounting for 16% of the variance, has minima nearly 180° apart (120°W – 180° and 30°W – 60°E) and a maximum centered in the Drake Passage. This bears a considerable resemblance to the second EOF of observed winter SIC (15% of the observed variance and shown as black contours on Fig. 7b). The two leading SIC modes in both the CCSM4 and the observations have spectral peaks near 4 yr (Figs. 7c,d), although caution should be used when comparing to the relatively short observational record (1979–2006). Additionally, EOFs 1 and 2 are significantly correlated in both the model and in the observations at ± 1 -yr lag (Fig. 7d), with the spatial pattern in Fig. 7a leading that in Fig. 7b by 1 yr.

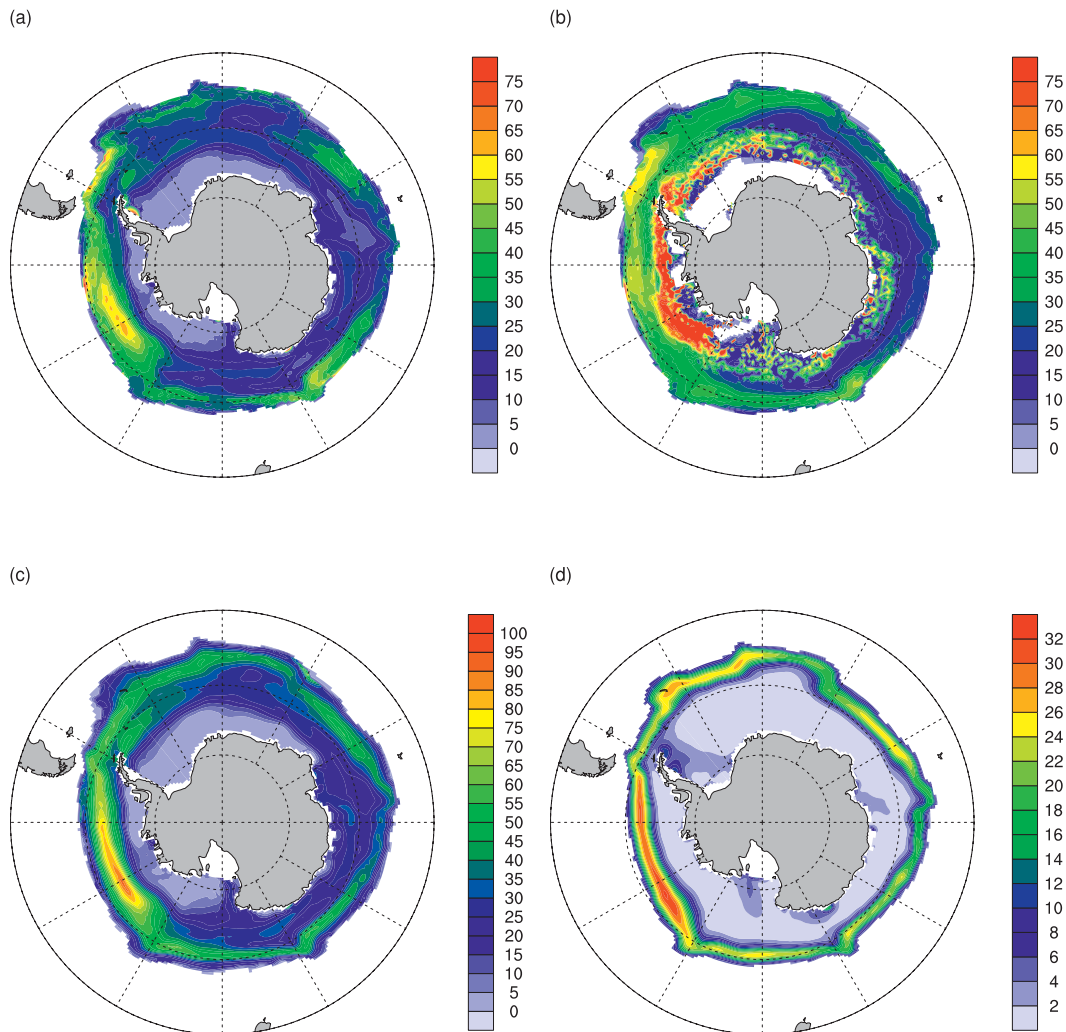


FIG. 6. CCSM4 control run standard deviations in (a) day of ice advance, (b) day of ice retreat, (c) total days above 15% SIC threshold, and (d) SIC (%).

The high correlation of the two leading SIC EOFs at 1-yr lag suggests that the second EOF may represent an eastward propagation of the first EOF. Eastward propagation of the anomalies is corroborated by the correlation of SIC PC1 with sea ice area (SIA is the total area of sea ice, computed by multiplying the SIC by the area of the grid cell and summing over that longitude) as a function of longitude and lag (Fig. 8). Wintertime SIC anomalies diminish significantly as they travel east, often barely detectable by 100°E in the middle to eastern section of the Indian Ocean. The anomalies, if they persisted, would take about 8 yr to travel around the globe, traveling at about $7\text{--}8\text{ cm s}^{-1}$ —time scales consistent both with modeled mean surface ocean current patterns and the eastward propagation of observations in the Antarctic circumpolar wave (White and Simmonds 2006). This suggests that the sea ice anomalies are in

effect advected with the mean ocean circulation. Although the regions of high SIC variability are in areas where the seasonal ice melts and is gone during austral summer, the ice anomaly is seen again in following years because of the corresponding anomalies in ocean SST—essentially a “memory” of the ice anomaly maintained in the surface ocean.

This is supported by an examination of both the surface temperature (TS—defined as the SST in ice-free regions and the ice surface temperature when ice covered) and the depth-integrated (to 100 m) ocean temperature variability in the region. Annual variations are examined for simplicity, although similar qualitative relationships are present for seasonal averages. The leading two annual TS EOFs (accounting for 25% and 12%, respectively, of the total variance) along with the power spectra of their associated PCs and correlations

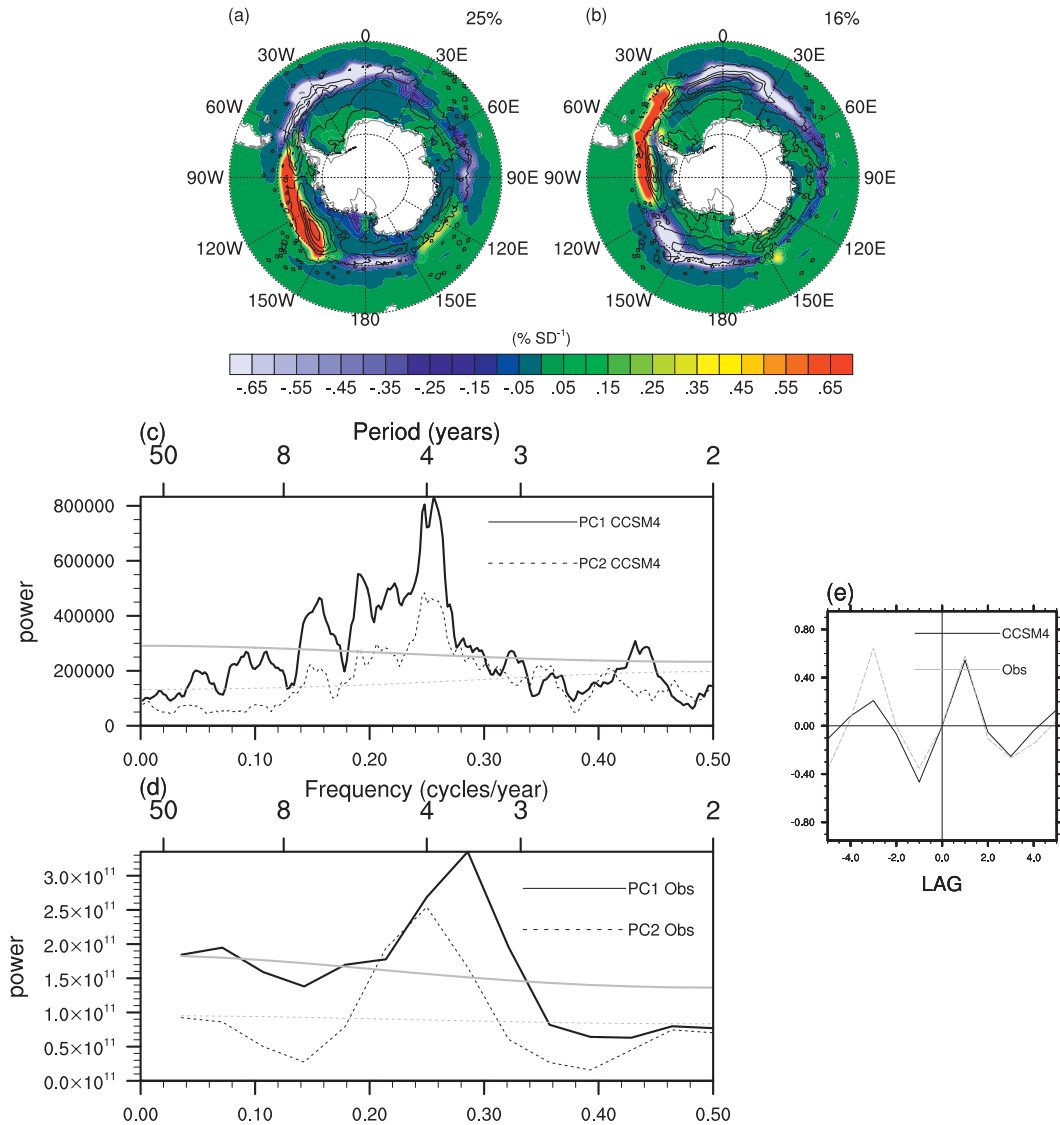


FIG. 7. Wintertime (JAS) SIC (a) EOF1 (b) EOF2, PC power spectra (gray lines indicate 95% confidence level) for (c) the CCSM4 and (d) the observations, and (e) correlations of PC1 and PC2 in the CCSM4 (black) and observations (gray). PC1 leads PC2 in the correlation. The black contours in (a),(b) show the corresponding EOFs from observed SIC (Comiso 1990, updated).

with first PC of wintertime SIC are shown in Fig. 9. The leading two EOFs of integrated ocean temperature, their spectra, and correlations with SIC are consistent with those of TS and are therefore not shown. The first two EOFs of annual TS are highly correlated (not shown) at ± 1 -yr lag, suggesting that like SIC, TS anomalies are propagating. The high correlation between the annual TS EOFs and the SIC EOFs ($r \sim 0.9$ for the first two PCs at 0 lag, and 0.6 for the second two) further reinforces the coupling between SIC and surface temperatures: the memory of the ice anomaly from one winter is maintained in surface ocean temperatures and advected

eastward, whereupon the anomaly propagates into the next winter (seen as the second EOF). As with the SIC variations, a dominant time period of about 4 yr is clearly evident.

To summarize, the dominant variability of Antarctic SIC in CCSM4 is characterized by a dipole pattern between the Pacific and Atlantic sectors that then propagates eastward. Although the Pacific anomaly propagates through the Drake Passage and into the Atlantic, both anomalies diminish significantly by the Indian Sector (near 100°E). These winter ice anomalies are tightly coupled to the SST variations, which provide an

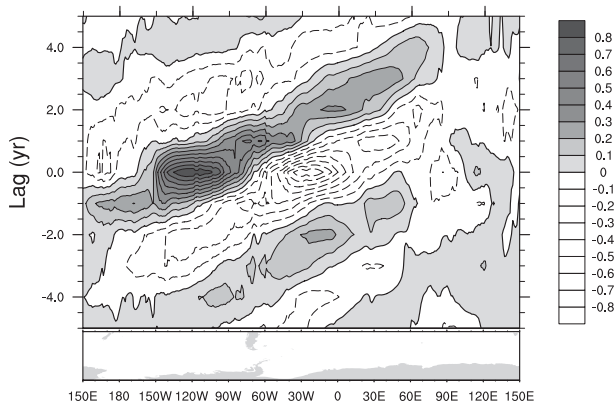


FIG. 8. Correlation of longitudinal sea ice area and the winter-time SIC PC1 as a function of longitude and lag (yr). The continental outlines are shown below for reference.

interannual memory and allows the winter ice cover variations to reoccur from one year to the next. A dipole signature in the SIC and TS fields are also seen in the observations (e.g., Yuan and Martinson 2001; Cai and Baines 2001; Gloersen and White 2001; Connolley

2003). Observational evidence suggests similar propagating anomalies associated with the Antarctic circumpolar wave (e.g., White and Peterson 1996; Connolley 2003) that are retained through the ice-free season by a similar oceanic mechanism (Gloersen and White 2001). This similarity to observations suggests that, even though the mean Antarctic sea ice extent is quite biased in CCSM4, the variability and its driving processes are well simulated. However, note that the biased ice extent does cause the variations in sea ice to occur equatorward of the observed anomalies and may influence aspects of the anomaly propagation.

A dipole pattern of SIC anomalies was also present in both the CCSM2 (Holland et al. 2005) and CCSM3 simulations (Holland and Raphael 2006); however, they propagate further and faster in CCSM4 than they did in CCSM2. EOF1 of SIC in CCSM4 is shifted a bit eastward compared with that of CCSM3, and they propagate at similar speeds and distances in both CCSM3 and CCSM4.

The third- and fourth-order EOFs for SIC (not shown here), representing 10% and 8% of the total variance,

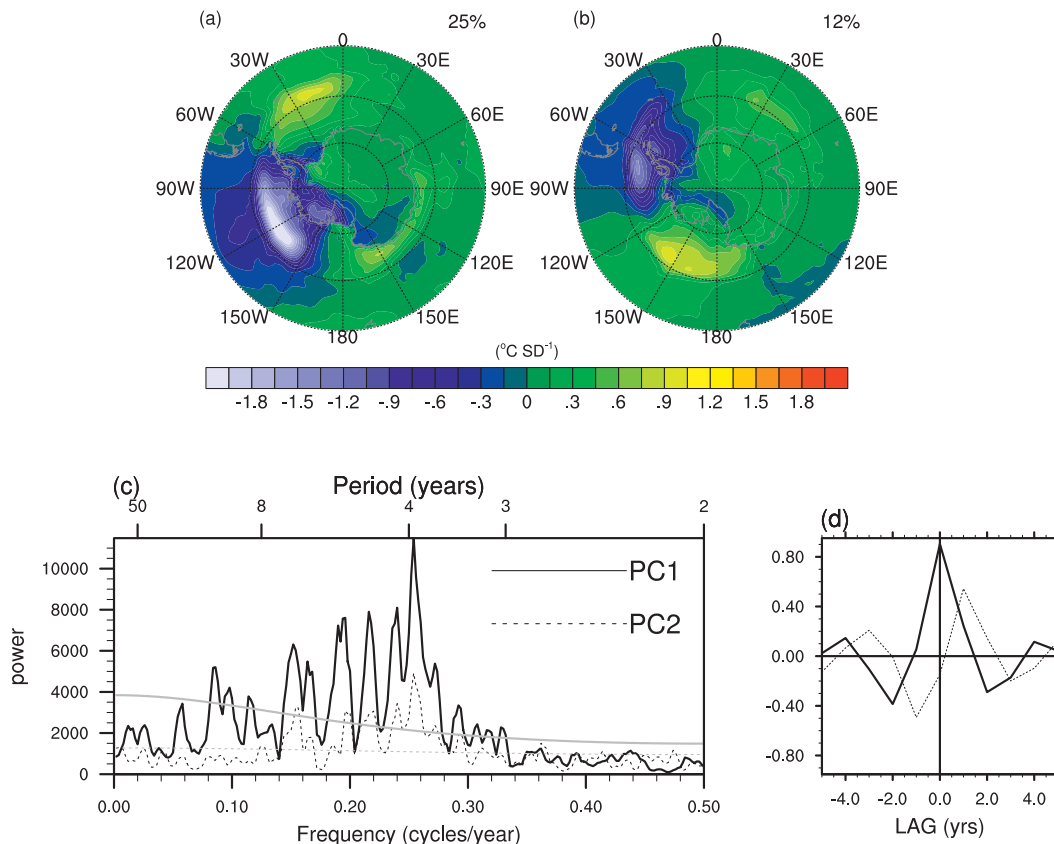


FIG. 9. CCSM4 control run annual TS (a) EOF1, (b) EOF2, (c) PC power spectra (gray lines indicate 95% confidence level), and (d) correlations of TS PC1 (solid) and TS PC2 (dashed) with the PC1 of JAS SIC. JAS SIC PC leads TS PCs in the correlations.

show a wave-3 pattern. Because they represent only a modest fraction of the variance, we focus on the first two EOFs and the factors that influence these leading patterns throughout this manuscript.

b. Factors contributing to the simulated SIC variability

Variability in the timing of ice advance as well as the leading SIC EOF dipole pattern suggests that there may be regionally different processes contributing to the seasonal ice concentration variability. For example, the location of the minimum sea level pressure around the Antarctic continent—the circumpolar trough (CPT)—influences both meridional and zonal circulation. Observations suggest that the location of the sea ice edge with respect to the CPT changes both seasonally and regionally, and spatial and temporal variability in the CPT affects the timing of the sea ice advance and retreat (e.g., Harangozo 2000; Stammerjohn et al. 2003; Simmonds et al. 2005). ENSO-modulated teleconnections lead to anomalies in SSTs, SLP, storm tracks, and intensities in the Southern Hemisphere, particularly in the Pacific (e.g., White and Peterson 1996; Peterson and White 1998; Yuan and Martinson 2001; Liu et al. 2002; White and Simmonds 2006). These oceanic and atmospheric anomalies affect ice area both dynamically and thermodynamically.

Ice area variations result from thermodynamic processes, including melt and growth anomalies, and dynamic processes associated with anomalous ice transport and ridging. The model computes and saves the ice area tendency terms because of these processes at each grid cell. More specifically, the sea ice model includes a subgrid-scale ice thickness distribution (ITD; Thorndike et al. 1975) with five ice categories governed by

$$\frac{\partial g}{\partial t} = -\frac{\partial}{\partial h}(fg) + L(g) - \mathbf{V} \cdot (\mathbf{v}g) + \Psi(h, g, \mathbf{v}), \quad (1)$$

where h is the ice thickness, f is the rate of change of ice thickness due to thermodynamic processes (melt and/or growth), $L(g)$ accounts for lateral melting, \mathbf{v} is the two-dimensional ice velocity, Ψ is the redistribution function that accounts for ridging and rafting, and g is the ice thickness distribution with $g(h)dh$ defined as the fractional area covered by ice of thickness h to $h + dh$, and $\Sigma g(h)dh$, over the five ice categories equals the total ice fraction within a grid cell (for more details see Hunke and Lipscomb 2008). For the ice area tendency computations, the thermodynamic tendency term includes the first two terms on the rhs of Eq. (1) summed over the ice categories, accounting for ice area changes resulting from all melt/growth effects (including basal, surface, and

lateral melt/growth). The dynamic ice area tendency term is the total of the last two terms on the rhs of Eq. (1) summed over the ice categories and so includes ice advective and mechanical redistribution effects.

To investigate the relationship of these terms with the leading winter ice variability, we compute area-weighted averages of the dynamic and thermodynamic ice area tendency variables for Pacific (180°–65°E) and Atlantic (65°W–30°E) regions corresponding to the maximum leading order wintertime SIC EOF anomalies. These regions are further constrained to areas where the variability in SIC associated with the first EOF is greater than $\pm 10\%$. We calculate correlation coefficients between the resulting monthly time series of thermodynamic and dynamic ice area tendency terms and the leading wintertime SIC PC (Fig. 10).

In the Pacific, positive ice concentration anomalies are associated with the first winter SIC EOF. The sea ice generally starts to advance into this region in April at which time positive correlations of the thermodynamic ice area tendency terms occur (Fig. 10a). This suggests that increased net ice growth (growth melt) in the region largely drives the wintertime SIC anomalies. Positive but much smaller correlations of dynamically driven ice area anomalies are also present in April suggesting that enhanced ice transport into the region reinforces the thermodynamic tendencies. These positive correlations are consistent with an approximately 40-day-earlier ice advance into the region (not shown) as diagnosed from regression analysis. The positive ice area tendency term correlations continue and reinforce the anomalous ice concentration through the fall and into the winter. From September through December, anomalously large ice loss from the region through dynamic processes is indicated by the negative correlations in Fig. 10a. This is a response to the positive wintertime SIC anomaly that allows enhanced transport from the region.

In the Atlantic sector, where negative SIC anomalies are associated with the first wintertime EOF, the correlation analysis (Fig. 10b) suggests that dynamically driven ice area anomalies play a larger role in the ice variability as compared to the anomalies in the Pacific. As the ice advances in March and April, reduced transport of ice into the region is indicated by the negative correlation coefficients. This is initially compensated by less ice melt (and positive thermodynamic tendency correlations) presumably because less ice is present. However, by June, the thermodynamic and dynamic tendency correlations are both negative and of comparable size, suggesting that enhanced ice melt ultimately contributes to the negative winter sea ice variations. As for the Pacific, the ice area tendency terms in the following spring and summer respond to the leading mode associated sea ice conditions

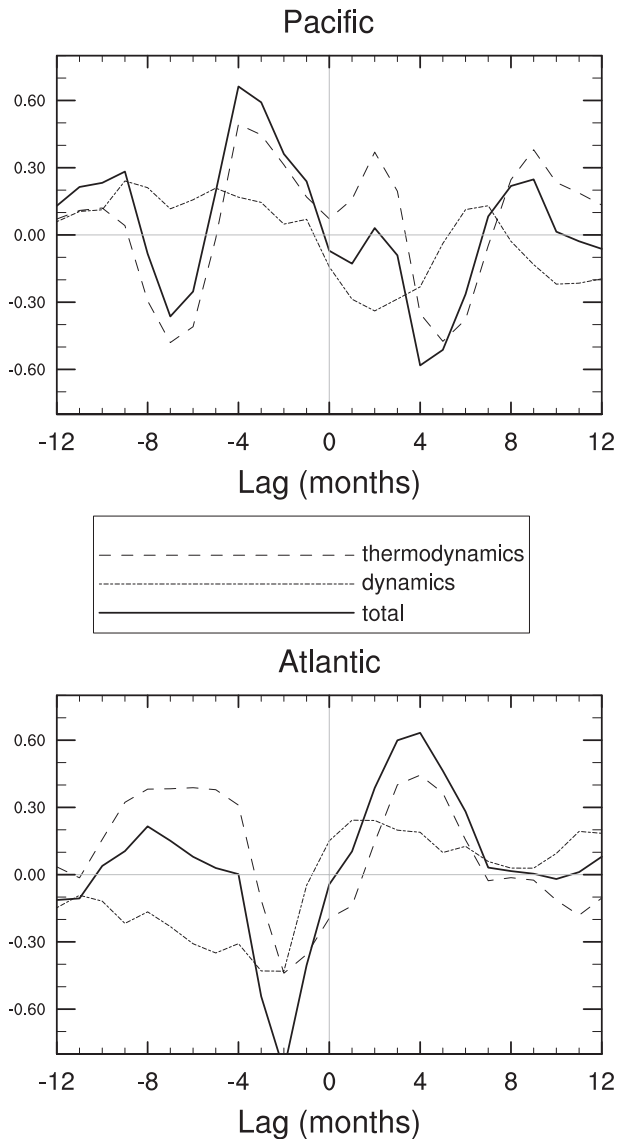


FIG. 10. Lagged correlations between wintertime SIC PC1 and (top) Pacific and (bottom) Atlantic monthly ice area tendencies. Negative lag means that the ice area tendency terms lead the SIC PC1.

and positive correlations for both dynamic and thermodynamic tendency terms result.

c. The influence of atmospheric coupling on sea ice variability

As shown above, the Pacific SIC anomalies associated with the leading mode of wintertime ice variability are largely driven by thermodynamic processes, whereas the Atlantic anomalies have a larger dynamically driven component. This suggests that both variations in atmosphere heating and wind anomalies may be important driving mechanisms. As such, here we examine

atmospheric modes of variability and their interactions with the sea ice variations. Because observational and previous modeling studies suggest important influences of ENSO and SAM on Antarctic sea ice variability, we focus on the relationships with these modes of variability. We note that other aspects of Antarctic atmospheric variability, such as the SAO and ENSO modulation of the SAO, can also influence Antarctic sea ice (e.g., Enomoto and Ohmura 1990; Simmonds 2003; Stammerjohn et al. 2003). For more information on the ENSO simulation and extratropical modes of variability within CCSM4, see Deser et al. (2012).

1) EL NIÑO–SOUTHERN OSCILLATION

The El Niño–Southern Oscillation (ENSO) is the dominant mode of interannual climate variability on a global scale. The Pacific–South America (PSA) circulation pattern is the primary ENSO–South Pacific teleconnection. This wave train results in positive sea level pressure anomalies (with positive ENSO) over the Bellingshausen Sea and leads to corresponding reductions of the westerly winds, equatorward migration of the storm tracks west of the tip of South America, and increased/decreased poleward heat transport in the South Pacific/South Atlantic (e.g., Mo 2000; Yuan 2004; Fogt and Bromwich 2006; Moy et al. 2009). These changes in atmospheric circulation set up anomalies in both SST and ice fields (Yuan 2004; Stammerjohn et al. 2008).

To assess the effect of ENSO on Southern Ocean conditions, a regression analysis was performed. Multiple variables were regressed onto the monthly Niño-3.4 SST time series, which is a measure of ENSO variability (Fig. 11c). As seen by this regression analysis (Fig. 11c), anomalously high SLP in the Amundsen/Bellingshausen Sea is associated with positive ENSO anomalies, suggesting that CCSM4 is reasonably capturing the PSA teleconnection. Ice concentration and surface temperature anomalies are also related to ENSO variability exhibiting anomalies of opposite sign in the Atlantic and Pacific basins. The extensive sea ice and anomalously low TS in the Atlantic is consistent with both the dynamic and thermodynamic forcing associated with ENSO-related meridional wind anomalies. In the Pacific the maximum ENSO-related high surface temperature anomalies lie in a region (150° – 120° W) of anomalous northerly winds. This is consistent with enhanced poleward heat transport in the South Pacific. Low sea ice anomalies are also present in this region and extend to Drake Passage (where southerly wind anomalies are present). This eastward extension of the sea ice anomalies is likely related to the transport of anomalous sea ice conditions into this region. Regression maps of daily

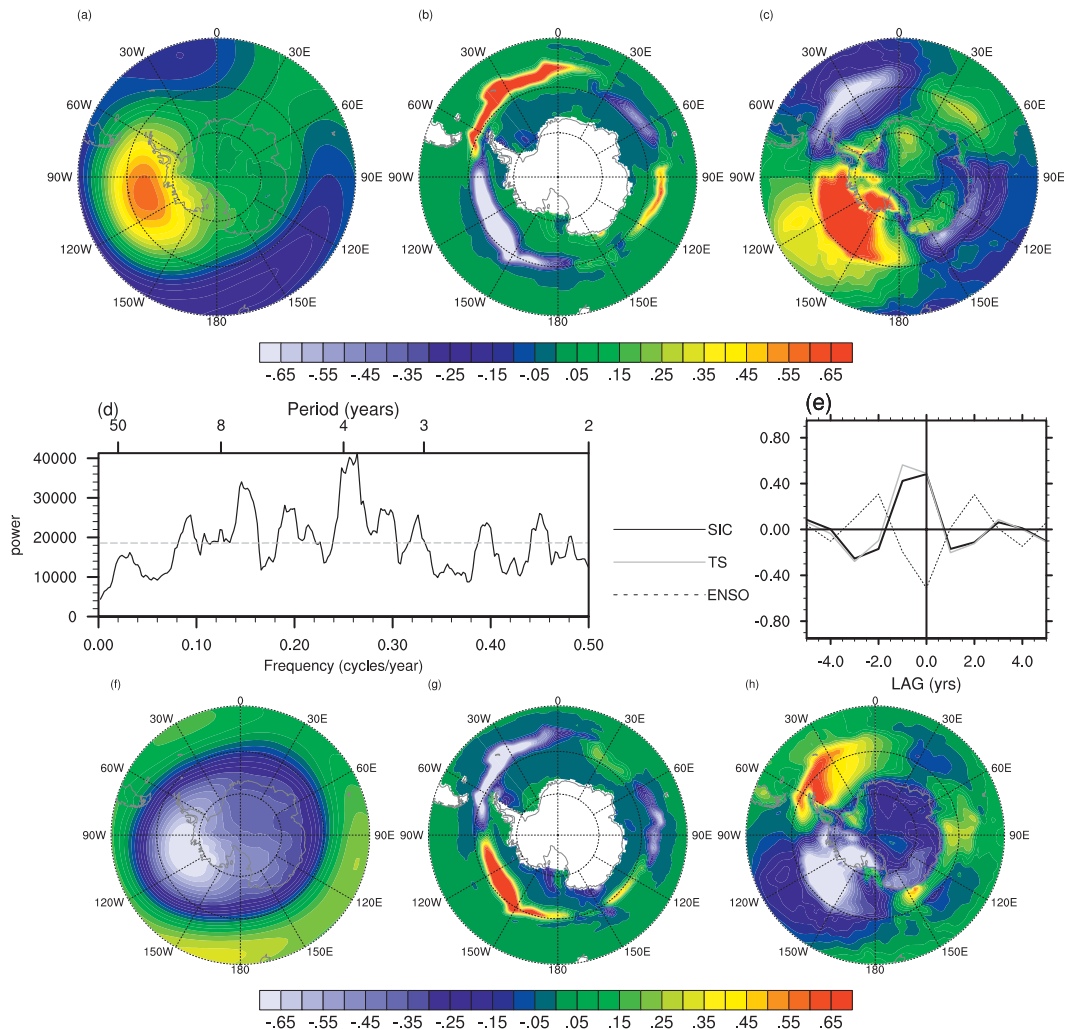


FIG. 11. CCSM4 control run (a) annual SLP, (b) JAS SIC, and (c) annual TS regressed onto annual Niño-3.4; (d) SAM power spectrum and (e) correlations with SIC (solid black), TS PC1 (gray) and Niño-3.4 (dashed); and (f) annual SLP, (g) JAS SIC, and (h) annual TS regressed on annual SAM. Variables in regression plots have been scaled to utilize the same contour color scale and are in units $\text{hPa} \times 4$ (SLP), $\% \times 0.1$ (SIC), and $^{\circ}\text{C}$ (TS).

ice advance/retreat on ENSO (Fig. 12) indicate that modeled ENSO strongly influences the ice advance and ice duration in agreement with observations (Stammerjohn et al. 2008).

The ENSO-related sea ice and surface temperature anomalies bear a very strong resemblance to the first EOF of winter sea ice cover (Fig. 7) and indeed the time series of the two are correlated at $R = -0.75$ (DJF Niño-3.4 at 0 lag). This explains the dominant 4-yr spectral peak in the leading sea ice mode variability in that ENSO has a dominant time period of 4 yr.

2) SOUTHERN ANNULAR MODE

SAM is the leading mode of atmospheric variability in the Southern Hemisphere. There are different definitions

of SAM, and they give similar results; for this paper we define SAM as the dominant empirical orthogonal function of sea level pressure south of 20°S (to exclude tropical variability). Positive SAM corresponds to negative SLP anomalies at high latitudes, positive SLP anomalies in midlatitudes, and strengthening of the westerly winds (Thompson and Wallace 2000). The SAM SLP anomaly is slightly asymmetric, with highest negative SLPs over West Antarctica/Bellingshausen Sea and leads to corresponding anomalies in meridional winds. Previous observational studies suggest that this asymmetry is in part due to the interaction of SAM variability and ENSO teleconnections in the South Pacific region (Fan 2007).

To assess the SAM–sea ice relationships in CCSM4, a SAM index is computed from an EOF analysis of

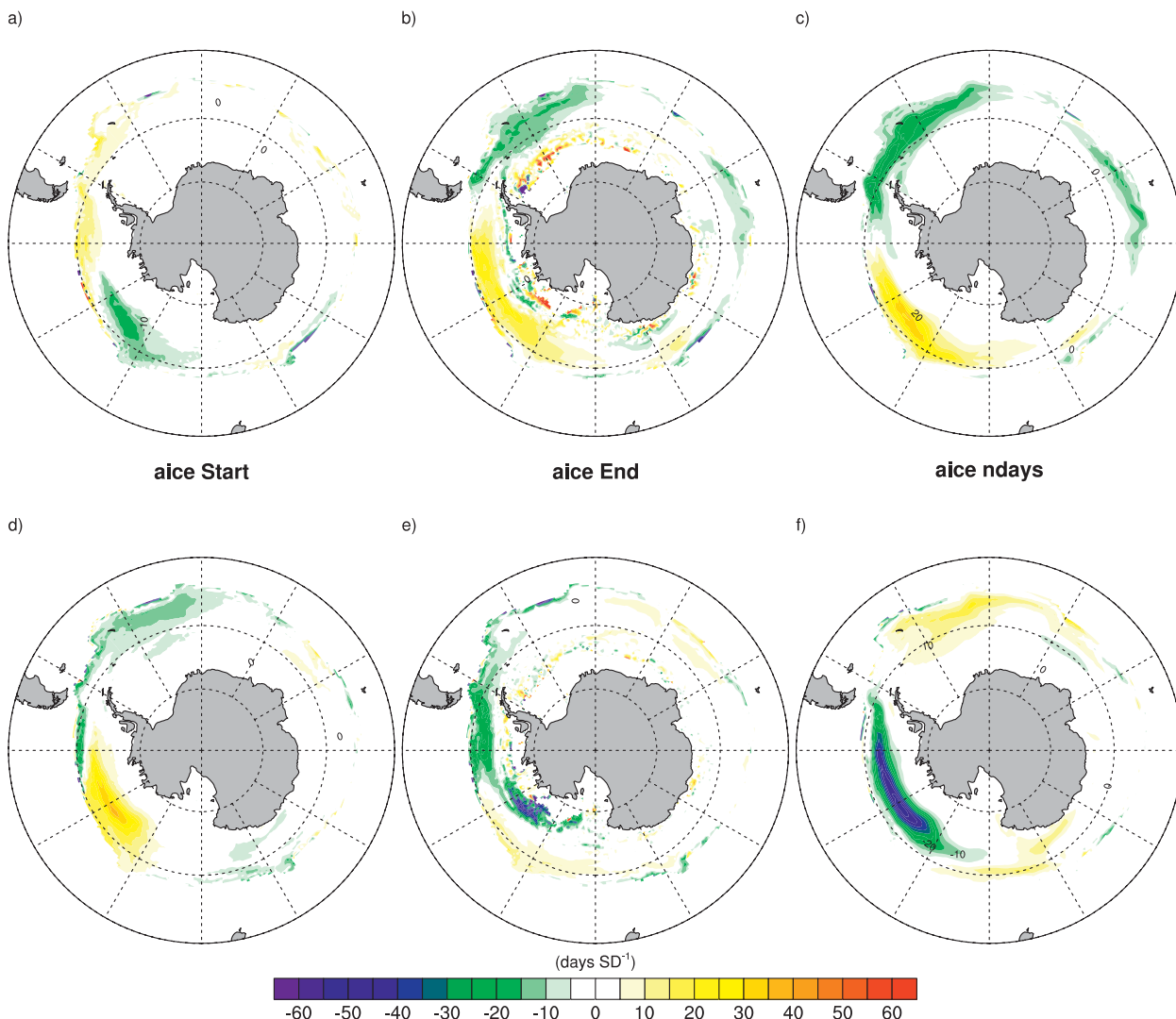


FIG. 12. Regressions of (a),(d) day of ice advance, (b),(e) day of ice retreat, and (c),(f) ice cover duration on (a)–(c) SAM and (d)–(f) Niño-3.4 indices.

annual average SLP values. Comparisons of annual and seasonal calculations of SAM indicate that the leading SLP EOF is very similar in all seasons, with the highest correlation found between annual SLP and wintertime ice extent at zero lag (Fig. 11b). SAM accounts for 41% of the variance in the control run annual SLP (the second EOF, not shown, accounts for 13% of the variance).

The SLP anomalies associated with SAM are well simulated compared to observations (Thompson and Wallace 2000; Hall and Visbeck 2002; Yuan and Li 2008; Fig. 11a). As with ENSO, the SAM variability projects onto SLP anomalies in the Bellingshausen/Amundsen Sea region but with an opposite sign. Not surprisingly, this results in SAM-related sea ice and surface temperature anomalies that are broadly similar (although

opposite in sign) to the anomalous surface conditions associated with ENSO. As with ENSO, SAM variability is highly correlated to the first EOF of wintertime SIC ($R = 0.48$).

Although the ENSO and SAM related sea ice variations are similar, some differences do exist. The relationship to the timing of sea ice advance and retreat is different between SAM and ENSO, with SAM having a stronger relationship to the timing of ice retreat and ENSO a stronger link to the timing of ice advance (Fig. 12). This may be related to different mechanisms forcing the ENSO- and SAM-related sea ice variations or a different timing of the important linkages, but a further investigation of these mechanisms is beyond the scope of this study.

5. Twentieth-century change

In the twentieth-century simulations, the Antarctic (60° – 90° S) surface temperature increases by about 1.2°C , and the SIA decreases by about 10%–15% from 1900 to 2005 (Fig. 13). These changes have similar timing, being most pronounced from 1960 onward, paralleling the rise in globally and hemispherically averaged temperatures and increasing external forcing of the climate system (e.g., Meehl et al. 2012). All of the ensemble members exhibit statistically significant (at 95% or higher confidence) increases in temperatures and decreases in SIA over 1960–2005 (Table 1), and the time series of surface temperature and sea ice area are anticorrelated with each other.

Most, but not all, Antarctic temperature datasets exhibit significant Antarctic-wide warming trends on the order of $0.1^{\circ}\text{C decade}^{-1}$ over the past 40–50 yr (Schneider et al. 2011). The trend in GISTEMP (Table 1) is significant and well within the range of trends in other datasets (Schneider et al. 2011). However, modeled trends in individual members and the ensemble mean are significantly greater (Table 1). For sea ice, there is limited observational and proxy evidence that sea ice extent in some sectors of the Antarctic in some seasons was greater earlier in the twentieth century than it is today (e.g., Rayner et al. 2003; Ackley et al. 2003; Curran et al. 2003; Goosse et al. 2009; de la Mare 2009). However, the information is sparse and the close association of Antarctic surface temperature and SIA suggests that the model also overestimates the trends in SIA.

The observed SAM index has increased significantly since the 1960s (Marshall 2003). The trend is statistically significant annually but is most pronounced in the austral summer (Marshall 2007). Both observations (e.g., Thompson and Solomon 2002; Marshall 2003; Schneider et al. 2004; Marshall 2007) and our model results (Fig. 11) indicate that the positive phase of the SAM is associated with negative temperature anomalies over most of the Antarctic continent, except in the Peninsula region. Given this relationship, the positive SAM trend has been invoked as an explanation for the relatively modest late twentieth-century rise in Antarctic temperatures, especially in austral summer and autumn (e.g., Thompson and Solomon 2002; Turner et al. 2005; Schneider et al. 2011) and also as a cause of the increase in Antarctic sea ice extent, notably in the Ross Sea (Turner et al. 2009). Therefore, if the model underestimates the SAM trend, it may overestimate Antarctic warming and sea ice loss. However, the CCSM4 results do not support this assertion. The majority of ensemble members do indeed indicate positive annual and austral

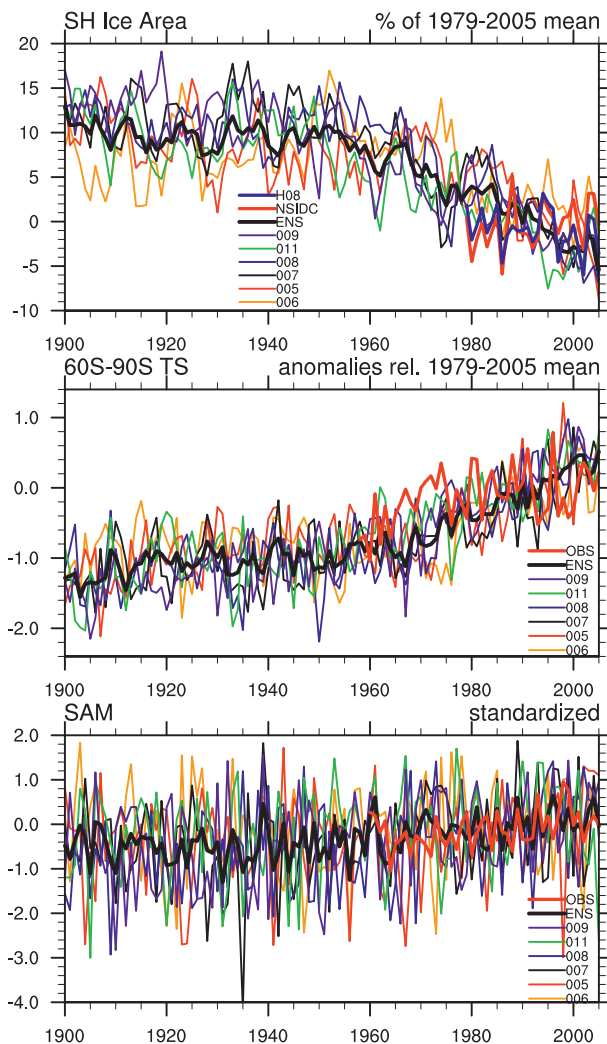


FIG. 13. Time series of annual anomalies of (top) Southern Hemisphere sea ice area, (middle) surface temperature for 60° – 90° S, and (bottom) the SAM index. The sea ice area and surface temperature time series are expressed as anomalies relative to the 1979–2005 mean for each CCSM4 ensemble member, ensemble mean, or observational index individually. The observed SAM index is from Marshall (2003) and was scaled to have the same variance and mean as the ensemble mean SAM index. Two sea ice area time series are shown, one is the sea ice index of NSIDC (Fetterer et al. 2009) and the other is from the dataset of Hurrell et al. (2008), marked H08 in the graph.

summer SAM trends over 1960–2005, statistically significant in one ensemble member and in the ensemble mean (Table 1). Comparing standardized time series, the rates of the observed and simulated SAM trends are statistically indistinguishable (Table 1 and Fig. 13). The question of whether the late twentieth-century SAM trend is exceptional compared to natural variability is beyond the scope of this study, but given the large variability evident in the time series of the SAM index, the

TABLE 1. Decadal trends and their 95% confidence intervals in annual sea ice area for the SH, annual surface air temperature (SAT) for 60°–90°S, and the annual and austral summer SAM indices for 1960–2005 simulated by each ensemble member (as numbered), the ensemble mean (ENS) and observed (OBS). Boldface numbers indicate trends significant at the 95% level. The observed SAT is from the GISTEMP analysis, the SAM index is from Marshall (2003), and the sea ice area is from the sea ice index of NSIDC (Fetterer et al. 2009). The Marshall index was scaled to have same variance as ensemble mean.

	Annual sea ice area (10 ⁶ km ² decade ⁻¹)	Annual SAT (°C decade ⁻¹)	Annual SAM (std dev decade ⁻¹)	Summer SAM (std dev decade ⁻¹)
006	–0.32 ± 0.18	0.31 ± 0.13	–0.05 ± 0.28	0.24 ± 0.30
005	–0.42 ± 0.23	0.35 ± 0.09	0.28 ± 0.23	0.27 ± 0.26
007	–0.40 ± 0.23	0.29 ± 0.10	0.08 ± 0.25	0.13 ± 0.26
008	–0.51 ± 0.22	0.36 ± 0.13	0.20 ± 0.24	0.21 ± 0.23
011	–0.31 ± 0.23	0.26 ± 0.11	–0.01 ± 0.27	0.21 ± 0.22
009	–0.32 ± 0.14	0.30 ± 0.08	0.12 ± 0.23	0.04 ± 0.27
ENS	–0.38 ± 0.08	0.31 ± 0.04	0.10 ± 0.09	0.18 ± 0.11
OBS	N/A	0.10 ± 0.08	0.11 ± 0.09	0.13 ± 0.12

modeled trend is clearly less exceptional than the simulated trends in sea ice area and surface temperature (Fig. 13). Nonetheless, numerous modeling studies have provided strong evidence that the positive SAM trend is associated with stratospheric ozone depletion (e.g., Gillett and Thompson 2003; Shindell and Schmidt 2004; Perlwitz et al. 2008) as well as greenhouse gas increases (e.g., Arblaster and Meehl 2006; Cai and Cowan 2007). The simulation of variability and trends in the SAM are strengths of the CCSM4 and its component atmospheric model, but this does not translate into sea ice and temperature trends that are similar to observations.

Using the period 1979–2005 permits additional comparisons of model results and observational data. In Fig. 14, zonally and monthly averaged changes (1996–2005 minus 1979–1987) in Antarctic sea ice area and temperature are compared for observations and the CCSM4 twentieth-century simulation. The observed trends are nuanced; cooling is evident in the first half of the calendar year, strongest in April, while warming is evident in the late austral winter and spring. On an annual basis, Antarctic-averaged temperature trends are not statistically significant for this time period (Table 2). Sea ice trends exhibit a similar seasonality as the temperature trends; increased sea ice trends are strongest in austral summer and autumn, while decreased sea ice trends are strongest in winter in spring. The observations also indicate that the 15% ice concentration contour has moved equatorward in autumn and poleward in late winter and early spring.

In contrast to the observed trends, the modeled ensemble-mean temperature and SIC trends are consistent throughout the year, showing sea ice loss and increasing temperatures year-round. The greatest relative changes in SIC occur near the northern ice edge, while weaker changes occur near the continent. The maximum temperature trends are collocated with the maximum sea ice trends and are strongest from April to June, an

obvious difference in seasonality compared to the observations. The largest temperature trends appear to lag the largest ice trends by about a month. For instance, the largest fractional ice loss occurs at about 65°S in March while at the same latitude the largest temperature increase occurs in April–May (Fig. 14). The temperature increase moves northward with the annual expansion of sea ice, an indication of coupling between the sea ice and temperature trends.

The spatial patterns of annual temperature, SIC, and SLP changes (1996–2005 minus 1979–1987) are compared in Fig. 15 for observations, the ensemble mean, and one ensemble member. The observations indicate pronounced warming in the Peninsula region and modest cooling trends in coastal East Antarctica from 100°E to 180°. Reductions in sea ice concentration of 30% or greater have occurred in the Bellingshausen Sea, while increases in SIC have occurred in the Ross Sea. A general drop in SLP is evident over the Antarctic, with the largest change of about 0.6 hPa near 70°S, 160°W.

The ensemble mean trends, compared to observations, are rather zonally symmetric. Sea ice loss is not concentrated in a particular longitudinal sector but instead occurs near the ice edge, where the CCSM4's mean ice extent is too far north (e.g., Fig. 5). As in the zonal mean case (Fig. 14), the largest temperature increases are collocated with the largest reductions in SIC. In the model, SLP also shows a general reduction over the Antarctic, but the changes are weaker in magnitude and more zonally symmetric than in nature. EOF analysis of SIC in the twentieth-century ensemble members (not shown) reveals a first or second EOF that resembles the ensemble mean pattern of change (Fig. 15). This trend pattern is distinct from the first and second EOFs of the control simulations discussed above, suggesting that the predominant trend pattern does not project onto SAM- or ENSO-related patterns of variability.

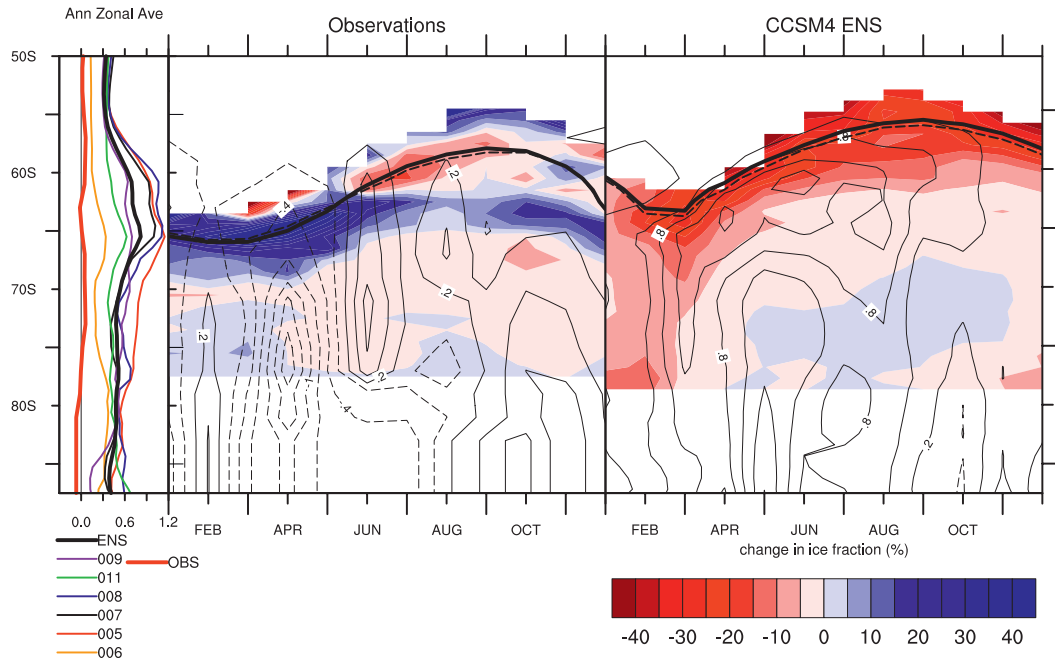


FIG. 14. Zonally averaged changes in sea ice fraction and surface temperature, expressed as the difference of the 1996–2005 and 1979–1987 time averages. (left) Annual zonally averaged surface temperature change for observations, the CCSM4 ensemble mean, and each ensemble member ($^{\circ}\text{C}$). (middle) Observed zonally averaged change by month for sea ice fraction (colors) and temperature (contours, interval = 0.3°C , negative contours dashed). Also shown is the mean latitude of the 15% ice fraction contour by month for the 1979–1987 time period (thick solid black line) and the 1996–2005 time period (thick dashed black line). (right) As in the middle panel, but for CCSM4 ensemble mean.

Results from a single ensemble member (member 006) compare more favorably to observations in that both gains and losses in SIC, and increases and decreases in temperatures, occur over the Antarctic (Fig. 15). As a consequence of the asymmetries in SIC changes and indicated in Table 2, the Antarctic-wide SIC trend in members 006 and 011 are not statistically significant for the 1979–2005 period, a result that is more similar to observations than the predominant trends over the longer time period (Fig. 13). While some studies have found a statistically significant increase in Antarctic sea ice extent and area (e.g., Cavalieri and Parkinson 2008;

Comiso and Nishio 2008), our analysis of the sea ice index suggests that the trend in sea ice area for 1979–2005 is not statistically significant (Table 2).

Table 2 suggests that there is not a relationship between the SAM trends and the modeled temperature and SAT trends among the ensemble members. The magnitudes of trends in SAT and SIA correspond to each other in the expected sense, that is, more warming is associated with greater reduction in SIA. However, the modeled SAM trends since 1979 are insignificant except for the ensemble mean in summer, and the members with insignificant SIA trends, 006 and 011,

TABLE 2. As in Table 1, but for 1979–2005.

	Annual sea ice area ($10^6 \text{ km}^2 \text{ decade}^{-1}$)	Annual SAT ($^{\circ}\text{C} \text{ decade}^{-1}$)	Annual SAM (std dev decade^{-1})	Summer SAM (std dev decade^{-1})
006	-0.06 ± 0.21	0.14 ± 0.20	-0.18 ± 0.56	-0.08 ± 0.56
005	-0.67 ± 0.37	0.42 ± 0.20	0.39 ± 0.59	0.50 ± 0.53
007	-0.66 ± 0.22	0.46 ± 0.21	0.18 ± 0.86	0.34 ± 0.65
008	-0.66 ± 0.37	0.40 ± 0.26	0.58 ± 0.60	0.31 ± 0.55
011	-0.31 ± 0.95	0.26 ± 0.20	-0.08 ± 0.55	0.24 ± 0.59
009	-0.47 ± 0.29	0.37 ± 0.19	0.19 ± 0.48	0.36 ± 0.80
ENS	-0.47 ± 0.10	0.34 ± 0.07	0.18 ± 0.28	0.28 ± 0.23
OBS	0.10 ± 0.12	0.00 ± 0.20	0.23 ± 0.23	0.22 ± 0.21

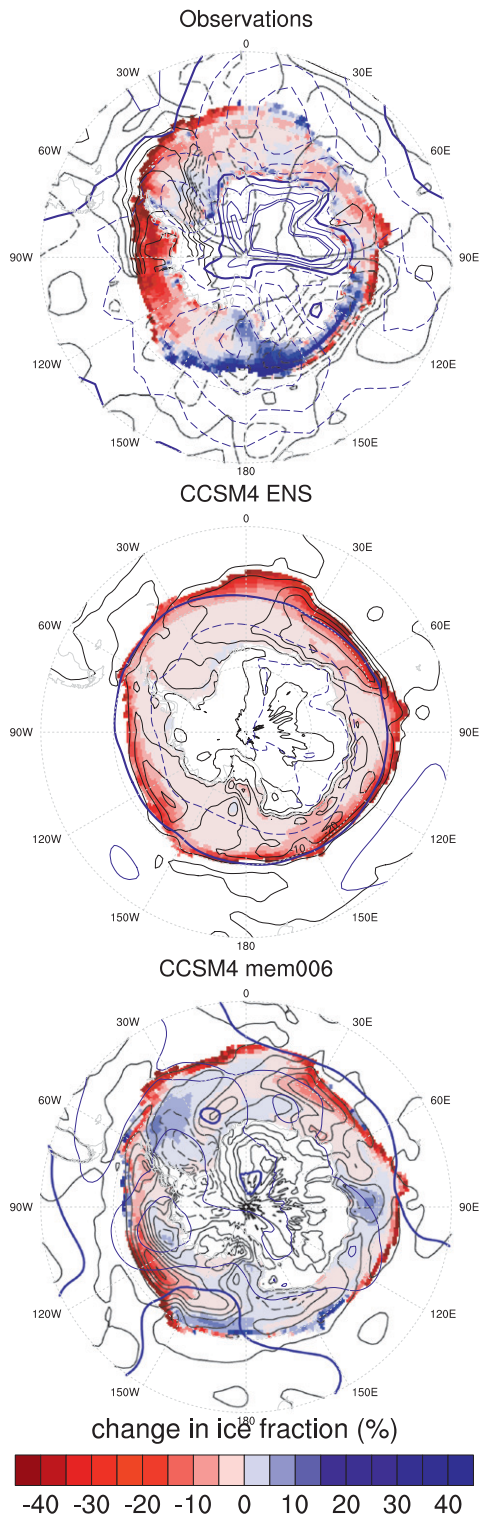


FIG. 15. Maps of 1996–2005 minus 1979–1987 changes in sea ice fraction (colors), sea level pressure (blue contours, interval = 0.2 hPa, positive contours solid and negative contours dashed) and surface temperature (black contours, interval = 0.2°C, positive contours solid and negative contours dashed) for (top) observations, (middle) CCSM4 ensemble mean, and (bottom) an individual ensemble member.

display SAM trends close to zero. This result seems counter to a commonly suggested explanation for increased Antarctic sea ice extent: changes in dynamic transport and equatorward Ekman currents resulting from increased zonal wind stress over the Southern Ocean (e.g., Hall and Visbeck 2002; Turner et al. 2009; Sigmund and Fyfe 2010). The model successfully captures the expected increase in wind stress associated with positive SAM (Fig. 16), but this mechanism alone cannot explain the sea ice trends. Sigmund and Fyfe (2010) found in experiments forced only with changes in stratospheric ozone depletion that increased wind stress and equatorward Ekman transport led to more ice production in summer but the effects on sea ice extent were counteracted by the ice edge meeting higher SSTs that shifted poleward and by increased upwelling of relatively warm circumpolar deepwater. Another explanation for increased Antarctic sea ice extent is an enhanced hydrological cycle (e.g., Liu and Curry 2010). However, neither explanation accounts for the marked regional contrasts in observed trends between the Amundesen–Bellingshausen and Ross Seas. Different mechanisms are likely needed to explain regionally differing modeled trends at the level of an ensemble member, such as 006.

Other evaluations of CCSM4 suggest possible explanations for the Antarctic-wide sea ice decrease and surface climate warming in the model ensemble mean. The warming of the Southern Ocean (e.g., Weijer et al. 2012) and of the global surface climate (Gent et al. 2011) are larger than observed and are consistent with the lack of representation in the CCSM4 of the indirect effects of aerosols [see Gent et al. (2011) for more discussion]. Associated with this excessive warming is a too large flux of shortwave radiation into the ocean and weak latent heat and sensible heat feedbacks acting on SST increases (Bates et al. 2012). As a result of these biases, the net downward longwave radiation increases more than would be expected for increasing greenhouse gases and ozone alone (Bates et al. 2012). Wind-driven changes in ocean circulation, such as those examined by Sigmund and Fyfe (2010), may also contribute to the simulated sea ice loss.

6. Conclusions

In contrast to the Arctic, where CCSM4 simulates very realistic sea ice (Jahn et al. 2012), the simulated Antarctic sea ice exhibits some major biases. The ice is too extensive in all months ranging from about 10 to 23 million km² over the annual cycle for the late twentieth-century ensemble mean, compared to an observed seasonal range of 3–19 million km². This is associated with

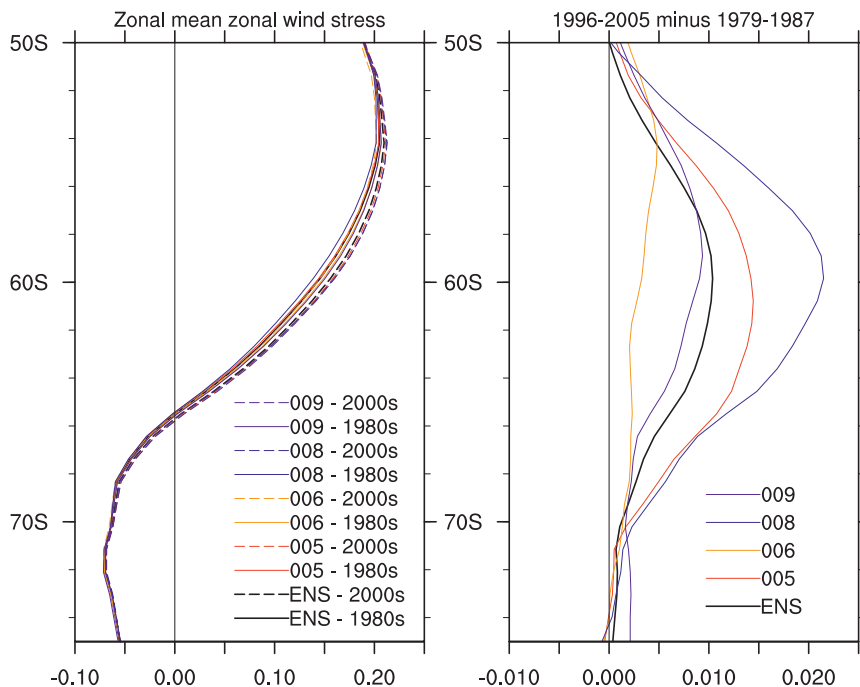


FIG. 16. Plots of zonal mean zonal wind stress (N m^{-2}). Climatologies for the 1960–69 and 1996–2005 time periods are compared for (left) four ensemble members and the ensemble mean of those members. (right) The differences of the two time periods are displayed.

thick sea ice and a large meridional transport, with implications for the sea ice mass budget and resulting ocean buoyancy fluxes. One likely culprit for these biases is the anomalously strong winds in the Southern Ocean, which contribute to enhanced equatorward Ekman transport of sea ice. Other factors of the coupled simulations, including cold SST bias in the Southern Ocean, also possibly contribute.

In spite of the biases in the mean sea ice cover, the wintertime ice variability shows considerable fidelity to observations. The leading mode of variability exhibits a dipole structure with anomalies of opposite sign in the Pacific and Atlantic and a significant 4-yr spectral peak. This pattern is advected eastward over multiple years with time scales consistent with the mean ocean currents. The anomalies reemerge over multiple years because of an imprint of the seasonal ice anomalies on the surface ocean conditions, finally dissipating near the Indian Ocean sector. The aspects of the sea ice variability bear considerable similarities to the Antarctic dipole and Antarctic circumpolar wave variations identified in observations (e.g., White and Peterson 1996; Yuan and Martinson 2000; Gloersen and White 2001).

The anomalies are driven by a combination of dynamic and thermodynamic changes in the ice cover. In the Pacific, thermodynamic processes (less ice melt) in the ice advance season play the dominant role in forcing the

positive ice anomalies. In the Atlantic, dynamic processes (less ice transport into the region) establish the anomalies and are then reinforced by ice melt variations. Both regions are strongly influenced by atmospheric conditions associated with ENSO and SAM, which both project onto SLP variability in the Bellingshausen–Amundsen Sea region. The dipole-like ice anomalies are consistent with the wind and atmospheric heat advection anomalies associated with these SLP variations. Interestingly, ENSO strongly correlates with the seasonal timing of ice advance in the Pacific and Atlantic ice anomaly regions, whereas SAM more strongly correlates with changes in the timing of ice retreat. This suggests that different seasonal processes are at work associated with ENSO and SAM. An influence of SAM and ENSO on the timing of Antarctic ice advance and retreat has also been seen in observations (Stammerjohn et al. 2008).

Over the twentieth century, the ensemble mean sea ice cover undergoes considerable reductions. The predominant pattern of sea ice change is roughly zonally symmetric with the largest reductions in SIC located near the sea ice edge and smallest reductions near the continent. Maximum temperature increases are collocated with the maximum changes in SIC. This pattern of change is consistent through the latter half of the twentieth century and not only for the 1979–2005 period of overlap with observations. However, as discussed

above, the SIC in the model exhibits considerable interannual variability, and as a consequence the latter twentieth-century trends in SIC are not always statistically significant for individual ensemble members. In the model, the predominant patterns of ice loss and temperature changes are distinct from the patterns of variability associated with SAM and ENSO. Observations suggest a less clear separation between trend patterns and patterns of variability, with combinations of persistent ENSO and SAM phases partly explaining the observed trends in Antarctic ice cover (Stammerjohn et al. 2008). Such phasing is not captured in free-running coupled model experiments, as phases of natural variability are not expected to coincide with those in nature.

The CCSM4 simulates realistic positive trends in the SAM, and associated trends in zonal mean zonal wind stress over the Southern Ocean. The effects on sea ice extent, however, are quite complex as discussed by Sigmond and Fyfe (2010), who showed that even if a model simulates SAM trends correctly, the sea ice can decrease because of factors other than Ekman transport. Whatever the mechanisms associated with the response to SAM, it is clear from our analysis that the Antarctic sea ice and air temperature trends are closely aligned. We argue that these trends likely reflect the stronger-than-observed warming of the surface oceans both globally (Bates et al. 2012) and in the Southern Ocean (Weijer et al. 2012) rather than the SAM.

CCSM4 biases in the mean Antarctic sea ice cover are a concern and can influence the Southern Ocean physical and biogeochemical simulations and likely the secular sea ice changes simulated by the model. Future model development efforts should address these Antarctic sea ice biases. As our analysis suggests that they result from coupled interactions (biases in winds, ice transport, and likely other properties), improvements may be required across multiple model components in order to improve the Antarctic sea ice simulation. In contrast, the good model representation of Antarctic sea ice variability, including the anomaly patterns and association to large-scale climate modes of variability, suggests that the model can be reliably used for some applications related to sea ice variability and its associated impacts.

Acknowledgments. Laura Landrum and D. Schneider were supported by grants from the National Science Foundation's Office of Polar Programs, Grants 0908675 and 0838871, respectively. The National Center for Atmospheric Research is sponsored by the National Science Foundation. We thank A. Phillips for processing much of the atmospheric model output analyzed here. We acknowledge the Computational and Information Systems Laboratory at NCAR, which provided computing

resources through the Climate Simulation Laboratory. Additionally, we thank the community of scientists and software engineers who have been instrumental in the development of CCSM4 and the helpful and constructive comments from the reviewers.

REFERENCES

- Ackley, S., P. Wadhams, J. Comiso, and A. Worby, 2003: Decadal decrease of Antarctic sea ice extent inferred from whaling records revisited on the basis of historical and modern sea ice records. *Polar Res.*, **22**, 19–25, doi:10.1111/j.1751-8369.2003.tb00091.x.
- Allan, R., and T. Ansell, 2006: A new globally complete monthly historical gridded mean sea level pressure dataset (HadSLP2): 1850–2004. *J. Climate*, **19**, 5816–5842.
- Ammann, C. M., G. A. Meehl, W. M. Washington, and C. Zender, 2003: A monthly and latitudinally varying volcanic forcing dataset in simulations of 20th century climate. *Geophys. Res. Lett.*, **30**, 1657, doi:10.1029/2003GL016875.
- Arblaster, J. M., and G. A. Meehl, 2006: Contributions of external forcings to southern annular mode trends. *J. Climate*, **19**, 2896–2905.
- Arrigo, K. R., G. L. van Dijken, and S. Bushinsky, 2008: Primary production in the Southern Ocean, 1997–2006. *J. Geophys. Res.*, **113**, C08004, doi:10.1029/2007JC004551.
- Bates, S. C., B. Fox-Kemper, S. R. Jayne, W. G. Large, S. Stevenson, and S. G. Yeager, 2012: Mean biases, variability, and trends in air–sea fluxes and sea surface temperature in the CCSM4. *J. Climate*, in press.
- Cai, W., and P. G. Baines, 2001: Forcing of the Antarctic circumpolar wave by El Niño–Southern Oscillation teleconnections. *J. Geophys. Res.*, **106** (C5), 9019–9038.
- , and T. Cowan, 2007: Trends in Southern Hemisphere circulation in IPCC AR4 models over 1950–99: Ozone depletion versus greenhouse forcing. *J. Climate*, **20**, 681–693.
- Cavalieri, D. J., and C. L. Parkinson, 2008: Antarctic sea ice variability and trends, 1979–2006. *J. Geophys. Res.*, **113**, C07004, doi:10.1029/2007JC004564.
- Collins, W. D., and Coauthors, 2006: The Community Climate System Model version 3 (CCSM3). *J. Climate*, **19**, 2122–2143.
- Comiso, J. C., 1990: DMSP SSM/I daily and monthly polar gridded bootstrap sea ice concentrations. National Snow and Ice Data Center, Boulder, CO, digital media. [Available online at <http://nsidc.org/data/nsidc-0002.html>.]
- , and F. Nishio, 2008: Trends in the sea ice cover using enhanced and compatible AMSR-E, SSM/I, and SMMR data. *J. Geophys. Res.*, **113**, C02S07, doi:10.1029/2007JC004257.
- Connolley, W. M., 2003: Long-term variation of the Antarctic circumpolar wave. *J. Geophys. Res.*, **107**, 8076, doi:10.1029/2000JC000380.
- Curran, M. A. J., T. D. van Ommen, V. I. Morgan, K. L. Phillips, and A. S. Palmer, 2003: Ice core evidence for Antarctic sea ice decline since the 1950s. *Science*, **302**, 1203–1206.
- Danabasoglu, G., S. Bates, B. P. Briegleb, S. R. Jayne, M. Jochum, W. G. Large, S. Peacock, and S. G. Yeager, 2012: The CCSM4 ocean component. *J. Climate*, **25**, 1361–1389.
- de la Mare, W. K., 2009: Changes in Antarctic sea-ice extent from direct historical observations and whaling records. *Climatic Change*, **92**, 461–493, doi:10.1007/s10584-008-9473-2.
- Deser, C., and Coauthors, 2012: ENSO and Pacific decadal variability in Community Climate System Model version 4. *J. Climate*, **25**, 2622–2651.

- Enomoto, H., and A. Ohmura, 1990: The influences of atmospheric half-yearly cycle on the sea ice extent in the Antarctic. *J. Geophys. Res.*, **95** (C6), 9497–9511.
- Fan, K., 2007: Zonal asymmetry of the Antarctic Oscillation. *Geophys. Res. Lett.*, **34**, L02706, doi:10.1029/2006GL028045.
- Fetterer, F., K. Knowles, W. Meier, and M. Savoie, 2009: Sea ice index. National Snow and Ice Data Center, Boulder, CO, digital media. [Available online at <http://nsidc.org/data/g02135.html>.]
- Fogt, R. L., and D. H. Bromwich, 2006: Decadal variability of the ENSO teleconnection to the high-latitude South Pacific governed by coupling with the southern annular mode. *J. Climate*, **19**, 979–997.
- Gent, P. R., and Coauthors, 2011: The Community Climate System Model version 4. *J. Climate*, **24**, 4973–4991.
- Gillett, N. P., and D. W. J. Thompson, 2003: Simulation of recent Southern Hemisphere climate change. *Science*, **302**, 273–275.
- Gloersen, P., and W. B. White, 2001: Reestablishing the circumpolar wave in sea ice around Antarctica from one winter to the next. *J. Geophys. Res.*, **106** (C3), 4391–4395.
- Goosse, H., W. Lefebvre, A. de Montety, E. Crespin, and A. H. Orsi, 2009: Consistent past half-century trends in the atmosphere, the sea ice and the ocean at high southern latitudes. *Climate Dyn.*, **33**, 999–1016, doi:10.1007/s00382-008-0500-9.
- Griffies, S. M., and Coauthors, 2009: Coordinated Ocean-Ice Reference Experiments (COREs). *Ocean Modell.*, **26**, 1–46, doi:10.1016/j.ocemod.2008.08.007.
- Hall, A., and M. Visbeck, 2002: Synchronous variability in the Southern Hemisphere atmosphere, sea ice, and ocean resulting from the annular mode. *J. Climate*, **15**, 3043–3057.
- Hansen, J., R. Ruedy, M. Sato, and K. Lo, 2010: Global surface temperature change. *Rev. Geophys.*, **48**, RG4004, doi:10.1029/2010RG000345.
- Harangozo, S. A., 1997: Atmospheric meridional circulation impacts on contrasting winter sea ice extent in two years in the Pacific sector of the Southern Ocean. *Tellus*, **49A**, 388–400.
- , 2000: A search for ENSO teleconnections in the West Antarctic Peninsula climate in austral winter. *Int. J. Climatol.*, **20**, 663–679.
- Harms, S., E. Fahrbach, and V. H. Strass, 2001: Sea ice transports in the Weddell Sea. *J. Geophys. Res.*, **106** (C5), 9057–9073.
- Holland, M. M., and M. N. Raphael, 2006: Twentieth century simulation of the Southern Hemisphere climate in coupled models. Part II: Sea ice conditions and variability. *Climate Dyn.*, **26**, 229–245, doi:10.1007/s00382-005-0087-3.
- , C. M. Bitz, and E. C. Hunk, 2005: Mechanisms forcing an Antarctic dipole in simulated sea ice and surface ocean conditions. *J. Climate*, **18**, 2051–2066.
- , D. A. Bailey, B. P. Briegleb, B. Light, and E. Hunke, 2012: Improved sea ice shortwave radiation physics in CCSM4: The impact of melt ponds and aerosols on Arctic sea ice. *J. Climate*, **25**, 1413–1430.
- Hunke, E. C., and W. H. Lipscomb, 2008: CICE: The Los Alamos Sea Ice Model, documentation and software, version 4.0. Los Alamos National Laboratory Tech. Rep. LA-CC-06-012, 76 pp.
- Hurrell, J. W., J. J. Hack, D. Shea, J. M. Caron, and J. Rosinski, 2008: A new sea surface temperature and sea ice boundary dataset for the Community Atmosphere Model 2008. *J. Climate*, **21**, 5145–5153.
- Jahn, A., and Coauthors, 2012: Late-twentieth-century simulation of Arctic sea ice and ocean properties in the CCSM4. *J. Climate*, **25**, 1431–1452.
- Kirkman, C. H., IV, and C. M. Bitz, 2010: The effect of the sea ice freshwater flux on Southern Ocean temperatures in CCSM3: Deep-ocean warming and delayed surface warming. *J. Climate*, **24**, 2224–2237.
- Lamarque, J.-F., and Coauthors, 2010: Historical (1850–2000) gridded anthropogenic and biomass burning emissions of reactive gases and aerosols: Methodology and application. *Atmos. Chem. Phys.*, **10**, 7017–7039, doi:10.5194/acp-10-7017-2010.
- , G. P. Kyle, M. Meinshausen, K. Riahi, S. J. Smith, D. P. van Vuuren, A. Conley, and F. Vitt, 2011: Global and regional evolution of short-lived radiatively-active gases and aerosols in the representative concentration pathways. *Climatic Change*, **109**, 191–212, doi:10.1007/s10584-011-0155-0.
- Large, W. G., and S. G. Yeager, 2009: The global climatology of an interannually varying air-sea flux data set. *Climate Dyn.*, **33**, 341–364, doi:10.1007/s00382-008-0441-3.
- Lawrence, D. M., K. W. Oleson, M. G. Flanner, C. G. Fletcher, P. J. Lawrence, S. Levis, S. C. Swenson, and G. B. Bonan, 2012: The CCSM4 land simulation, 1850–2005: Assessment of surface climate and new capabilities. *J. Climate*, **25**, 2240–2260.
- Lean, J., 2000: Evolution of the sun's spectral irradiance since the Maunder Minimum. *Geophys. Res. Lett.*, **27**, 2425–2428.
- Liu, J., and J. A. Curry, 2010: Accelerated warming of the Southern Ocean and its impacts on the hydrological cycle and sea ice. *Proc. Natl. Acad. Sci. USA*, **107**, 14 987–14 992, doi:10.1073/pnas.1003336107.
- , X. Yuan, D. Rind, and D. G. Martinson, 2002: Mechanism study of the ENSO and southern high latitude climate teleconnections. *Geophys. Res. Lett.*, **29**, 1679, doi:10.1029/2002GL015143.
- , J. A. Curry, and D. G. Martinson, 2004: Interpretation of recent Antarctic sea ice variability. *Geophys. Res. Lett.*, **31**, L02205, doi:10.1029/2003GL018732.
- Lo Monaco, C., N. Metzl, A. Poisson, C. Brunet, and B. Schauer, 2005: Anthropogenic CO₂ in the Southern Ocean: Distribution and inventory at the Indian–Atlantic boundary (World Ocean Circulation Experiment line I6). *J. Geophys. Res.*, **110**, C06010, doi:10.1029/2004JC002643.
- Marshall, G. J., 2003: Trends in the southern annular mode from observations and reanalyses. *J. Climate*, **16**, 4134–4143.
- , 2007: Half-century seasonal relationships between the southern annular mode and Antarctic temperatures. *Int. J. Climatol.*, **27**, 373–383.
- Meehl, G. A., and Coauthors, 2012: Climate system response to external forcings and climate change projections in CCSM4. *J. Climate*, **25**, 3661–3683.
- Mo, K. C., 2000: Relationships between low-frequency variability in the Southern Hemisphere and sea surface temperature anomalies. *J. Climate*, **13**, 3599–3610.
- Moy, C. M., P. I. Moreno, R. B. Dunbar, M. R. Kaplan, J. P. Francois, R. Villalba, and T. Haberzettl, 2009: Past climate variability in South America and surrounding regions. *Climate Change in Southern South America during the Last Two Millennia*, F. Vimeux et al., Eds., Springer, 353–393.
- North, G. N., T. L. Bell, and R. F. Cahalan, 1982: Sampling errors in the estimation of empirical orthogonal functions. *Mon. Wea. Rev.*, **110**, 699–706.
- Parkinson, C. L., 2002: Trends in the length of the Southern Ocean sea-ice season, 1979–99. *Ann. Glaciol.*, **34**, 435–440.
- Perlwitz, J., S. Pawson, R. L. Fogt, J. E. Nielsen, and W. D. Neff, 2008: Impact of stratospheric ozone hole recovery on Antarctic climate. *Geophys. Res. Lett.*, **35**, L08714, doi:10.1029/2008GL033317.

- Peterson, R. G., and W. B. White, 1998: Slow oceanic teleconnections linking the Antarctic circumpolar wave with the tropical El Niño–Southern Oscillation. *J. Geophys. Res.*, **103** (C11), 24 573–24 583.
- Raphael, M. N., and M. M. Holland, 2006: Twentieth century simulation of the Southern Hemisphere climate in coupled models. Part 1: Large scale circulation variability. *Climate Dyn.*, **26**, 217–228, doi:10.1007/s00382-005-0082-8.
- Rayner, N. A., D. E. Parker, E. B. Horton, C. K. Folland, L. V. Alexander, D. P. Rowell, E. C. Kent, and A. Kaplan, 2003: Global analyses of sea surface temperature, sea ice, and night marine air temperature since the late nineteenth century. *J. Geophys. Res.*, **108**, 4407, doi:10.1029/2002JD002670.
- Reynolds, R. W., N. A. Rayner, T. M. Smith, D. C. Stokes, and W. Q. Wang, 2002: An improved in situ and satellite SST analysis for climate. *J. Climate*, **15**, 1609–1625.
- Schneider, D. P., E. J. Steig, and J. C. Comiso, 2004: Recent climate variability in Antarctica from satellite-derived temperature data. *J. Climate*, **17**, 1569–1583.
- , C. Deser, and Y. Okumura, 2011: An assessment and interpretation of the observed warming of West Antarctica in the austral spring. *Climate Dyn.*, **38**, 323–347, doi:10.1007/s00382-010-0985-x.
- Sen Gupta, A., and M. H. England, 2006: Coupled ocean–atmosphere–ice response to variations in the southern annular mode. *J. Climate*, **19**, 4457–4486.
- Shields, C. A., D. A. Bailey, G. Danabasoglu, M. Jochum, J. T. Kiehl, S. Levis, and S. Park, 2012: The low-resolution CCSM4. *J. Climate*, **25**, 3993–4014.
- Shindell, D. T., and G. A. Schmidt, 2004: Southern Hemisphere climate response to ozone changes and greenhouse gas increases. *Geophys. Res. Lett.*, **31**, L18209, doi:10.1029/2004GL020724.
- Sigmond, M., and J. C. Fyfe, 2010: Has the ozone hole contributed to increased Antarctic sea ice extent? *Geophys. Res. Lett.*, **37**, L18502, doi:10.1029/2010GL044301.
- Simmonds, I., 2003: Modes of atmospheric variability over the Southern Ocean. *J. Geophys. Res.*, **108**, 8078, doi:10.1029/2000JC000542.
- , and T. H. Jacka, 1995: Relationships between the interannual variability of Antarctic sea ice and the Southern Oscillation. *J. Climate*, **8**, 637–647.
- , A. Rafter, T. Cowan, A. B. Watkins, and K. Keay, 2005: Large-scale vertical momentum, kinetic energy, and moisture fluxes in the Antarctic sea ice region. *Bound.-Layer Meteor.*, **117**, 149–177, doi:10.1007/s10546-004-5939-6.
- Smith, R. D., and Coauthors, 2010: The Parallel Ocean Program (POP) reference manual. Los Alamos National Laboratory Tech. Rep. LAUR-10-01853, 140 pp.
- Smith, W. O., and D. M. Nelson, 1985: Phytoplankton bloom produced by a receding ice edge in the Ross Sea: Spatial coherence with the density field. *Science*, **227**, 163–166, doi:10.1126/science.227.4683.163.
- Stammerjohn, S. E., M. R. Drinkwater, R. C. Smith, and X. Liu, 2003: Ice-atmosphere interactions during sea-ice advance and retreat in the western Antarctic Peninsula region. *J. Geophys. Res.*, **108**, 3329, doi:10.1029/2002JC001543.
- , D. G. Martinson, R. C. Smith, X. Yuan, and D. Rind, 2008: Trends in Antarctic annual sea ice retreat and advance and their relation to El Niño–Southern Oscillation and southern annular mode variability. *J. Geophys. Res.*, **113**, C03S90, doi:10.1029/2007JC004269.
- Takahashi, T., and Coauthors, 2002: Global sea-air CO₂ flux based on climatological surface ocean pCO₂, and seasonal biological and temperature effects. *Deep-Sea Res. II*, **49** (9–10), 1601–1622, doi:10.1016/S0967-0645(02)00003-6.
- Thompson, D. W. J., and J. M. Wallace, 2000: Annular modes in the extratropical circulation. Part I: Month-to-month variability. *J. Climate*, **13**, 1000–1016.
- , and S. Solomon, 2002: Interpretation of recent Southern Hemisphere climate change. *Science*, **296**, 895–899.
- Thorndike, A. S., D. A. Rothrock, G. A. Maykut, and R. Colony, 1975: The thickness distribution of sea ice. *J. Geophys. Res.*, **80** (33), 4501–4513.
- Turner, J., and Coauthors, 2004: The SCAR READER project: Toward a high-quality database of mean Antarctic meteorological observations. *J. Climate*, **17**, 2890–2898.
- , and Coauthors, 2005: Antarctic climate change during the last 50 years. *Int. J. Climatol.*, **25**, 279–294.
- , and Coauthors, 2009: Non-annular atmospheric circulation change induced by stratospheric ozone depletion and its role in the recent increase of Antarctic sea ice extent. *Geophys. Res. Lett.*, **36**, L08502, doi:10.1029/2009GL037524.
- van Loon, H., 1967: The half-yearly oscillations in middle and high southern latitudes and the coreless winter. *J. Atmos. Sci.*, **24**, 472–486.
- Vavrus, S., and D. Waliser, 2008: An improved parameterization for simulating Arctic cloud amount in the CCSM3 climate model. *J. Climate*, **21**, 5673–5687.
- Wang, Y.-M., J. L. Lean, and N. R. Sheeley Jr., 2005: Modeling the sun's magnetic field and irradiance since 1713. *Astrophys. J.*, **625**, 522–538.
- Weijer, W., and Coauthors, 2012: The Southern Ocean and its climate in CCSM4. *J. Climate*, **25**, 2652–2675.
- White, W. B., and R. G. Peterson, 1996: An Antarctic circumpolar wave in surface pressure, temperature, and sea-ice extent. *Nature*, **380**, 699–702.
- , and I. Simmonds, 2006: Sea surface temperature-induced cyclogenesis in the Antarctic circumpolar wave. *J. Geophys. Res.*, **111**, C08011, doi:10.1029/2004JC002395.
- Yuan, X., 2004: ENSO-related impacts on Antarctic sea ice: A synthesis of phenomenon and mechanisms. *Antarct. Sci.*, **16**, 415–425.
- , and D. G. Martinson, 2000: Antarctic sea ice extent variability and its global connectivity. *J. Climate*, **13**, 1697–1717.
- , and —, 2001: The Antarctic dipole and its predictability. *Geophys. Res. Lett.*, **28**, 3609–3612.
- , and C. Li, 2008: Climate modes in southern high latitudes and their impacts on Antarctic sea ice. *J. Geophys. Res.*, **113**, C06S91, doi:10.1029/2006JC004067.
- Zhang, J., 2007: Increasing Antarctic sea ice under warming atmospheric and oceanic conditions. *J. Climate*, **20**, 2515–2529.